BACHELOR THESIS · XLAS

Measuring heat fluxes over large distances

Patrick van den Hoek
4 June 2014

The Hague University Delft

Study:	Applied physics
Student number:	10009582
First Mentor Hague University:	Drs. M.C. Vloemans
Second Mentor Hague University:	Ing. J.L. van Yperen

Kipp & Zonen

Mentor Kipp & Zonen:	Dr. K.M. Wilson

Summary

Kipp & Zonen, based in Delft manufactures and develops atmospheric measurement instruments, including a scintillometer. Kipp & Zonen currently manufactures the large aperture scintillometer (LAS) MkII and previously manufactured the extra large aperture scintillometer (XLAS) MkI. A scintillometer can measure the sensible heat flux, the amount of warm rising warm due to the solar radiation. A LAS or XLAS consists of a transmitter and a receiver, measuring over a long open path. The XLAS, a scaled up version of the LAS, allows measurements over even longer paths up to 10 km, on the scale of satellite pixels or atmospheric models. In this bachelor thesis a XLAS MkII was built and tested and a LAS was compared with other scintillometers to verify the quality of the measurements.

The frequency spectrum was investigated to see if the scintillometers were responding to the typical scintillation spectrum. The frequency spectrum of a reference LAS, a control LAS, an upgraded old LAS and two XLAS were found similar to the typical spectrum. A LAS from Wageningen University, of different design, showed a strong noise spike.

A XLAS with a reduction ring in front of it was compared with a LAS. The reduction ring has the same aperture diameter as the aperture of the LAS, making the two instruments comparable. A LAS transmitter was placed on the roof of the University of Delft and receivers were placed on the roof of Kipp & Zonen. Reference LAS 120001, control LAS 120002, XLAS 140001 and 140002, were placed on the Kipp & Zonen roof. The measurements from the scintillometers were compared in the form of the structure parameter of the refractive index of air (C_{n}^2). Control LAS 120002 measured 2.8 ± 0.5 % higher C_{n}^2 than reference LAS 120001. The XLAS measured lower C_{n}^2 values than reference LAS 120001, 6.3 ± 0.7 % lower for XLAS 140001 and 4.2 ± 0.9 % lower for XLAS 140002. The two XLAS agreed very well, with XLAS 140002 measuring C_{n}^2 values 1.3 ± 0.9 % higher than XLAS 140001.

The Kipp & Zonen LAS was compared with a LAS developed by Wageningen University, with a reversed path. The Wageningen LAS transmitter was placed on the Kipp & Zonen roof and the Wageningen LAS receiver was placed on the TU Delft roof. The Wageningen LAS measured 23 ± 2 % higher C_{n}^2 than reference LAS 120001. This was due to a peak in the frequency spectrum, which leads to an offset in the measured C_{n}^2. This is probably due to noise from the electronics.

The Kipp & Zonen LAS was also compared with a LAS from Scintec (BLS900), replacing the Wageningen LAS again in a reversed path configuration. The BLS900 has a low pass filter of 150 Hz, as opposed to the Kipp & Zonen LAS 120001 and 120002, which have a band pass filter from 0.5 to 400 Hz. For this comparison LAS 040007 has a band pass filter set to 0.1 Hz to 400 Hz, which more closely matches the BLS900.
The BLS900 measures 8 ± 1 % higher C_{n}^2 than reference LAS 120001, and only 2 ± 1 % higher C_{n}^2 than LAS 040007 with the different band pass filter setting of 0.1 Hz to 400 Hz. If the band pass filter of LAS 040007 is changed back to 0.5 Hz to 400 Hz, to match, then the measured C_{n}^2 values agree extremely well with reference LAS 120001, within an uncertainty of 0.8 %.

To summarise, the Kipp & Zonen LAS agreed very well with each other and with the BLS900 if the same band pass filter range was used. The XLAS with a reduction ring agreed very well with the LAS.

Content

1 Introduction

Kipp & Zonen is a company, which provides class-leading instruments for measuring solar radiation and atmospheric properties. The department research and development engages in improving instruments and developing new instruments.

One of the instruments which measure atmospheric properties is the large aperture scintillometer. A scintillometer can measure the sensible heat flux, the amount of warm rising air due to the solar radiation. A scintillometer consists of a transmitter and receiver which can measure heat fluxes over a distance up to 5 kilometres. The measurement from the scintillometer cannot be compared well with the data from satellites, because satellites measure heat fluxes on a larger scale around 10 kilometres. An extra large aperture scintillometer has been developed to measure the sensible heat flux over longer distances up to 10 kilometres.
Kipp & Zonen currently manufacture an upgraded large aperture scintillometer with new electronics and digital output and manufactured an extra large aperture scintillometer with old design. Currently an extra large aperture scintillometer with new electronics is designed.

The goal of the internship is to,

- build two extra large aperture scintillometers
- measure the focal length of the lens, in order to align the optics
- test the transmitter and receiver
- compare the extra large aperture scintillometer with the large aperture scintillometer
- compare the large aperture scintillometer with the large aperture scintillometer from Wageningen
- compare the large aperture scintillometer with the large aperture scintillometer from Scintec
- test the extra large aperture scintillometer over a distance of 10 kilometres, to determine the range.

First the extra large aperture scintillometer will be assembled. Than the back plate containing the electronics will be tested and the focal length of the Fresnel lens will be measured. When the focal length is determined, the detector or the LED can be positioned at the focus of the lens, and the scintillometer optically aligned. By employing a reduction ring in front of it, the extra large aperture scintillometer will be compared with the large aperture scintillometer. The comparison will take place over a distance of 889 meters. Then in the same location the large aperture scintillometer will be compared with the large aperture scintillometer from Wageningen and will also been compared with the large aperture scintillometer of Scintec. Finally the extra large aperture scintillometer will be tested over a distance off 10 kilometres.

2 Scintillometers

In this chapter the theory behind scintillometers will be explained. In the first paragraph the earth's energy budget is explained. The second paragraph explains the heat fluxes. The third paragraph goes into detail about the method behind measuring scintillations. The fourth paragraph describes the transmitted signal and the received signal. In the fifth paragraph the importance of saturation of the signal is explained. Finally how the sensible heat flux can be calculated is explained in the sixth paragraph.

2.1 Earth's energy budget

The energy budget of the earth is determined by the net flow of the shortwave radiation onto the earth and the longwave radiation out into space. Figure 1 details the energy budget of the earth, which shows that 100 % of the incoming energy is coming from the sun. 30 % of this solar energy is reflected into space from the atmosphere, clouds and from the ground. 51 % of the solar energy is absorbed by the earth's surface. A part of this energy is transferred into evaporation of water (latent heat flux), heated rising air (sensible heat flux) and emission of longwave radiation. Also 19 % of the incoming solar energy is absorbed by the atmosphere and clouds [4].

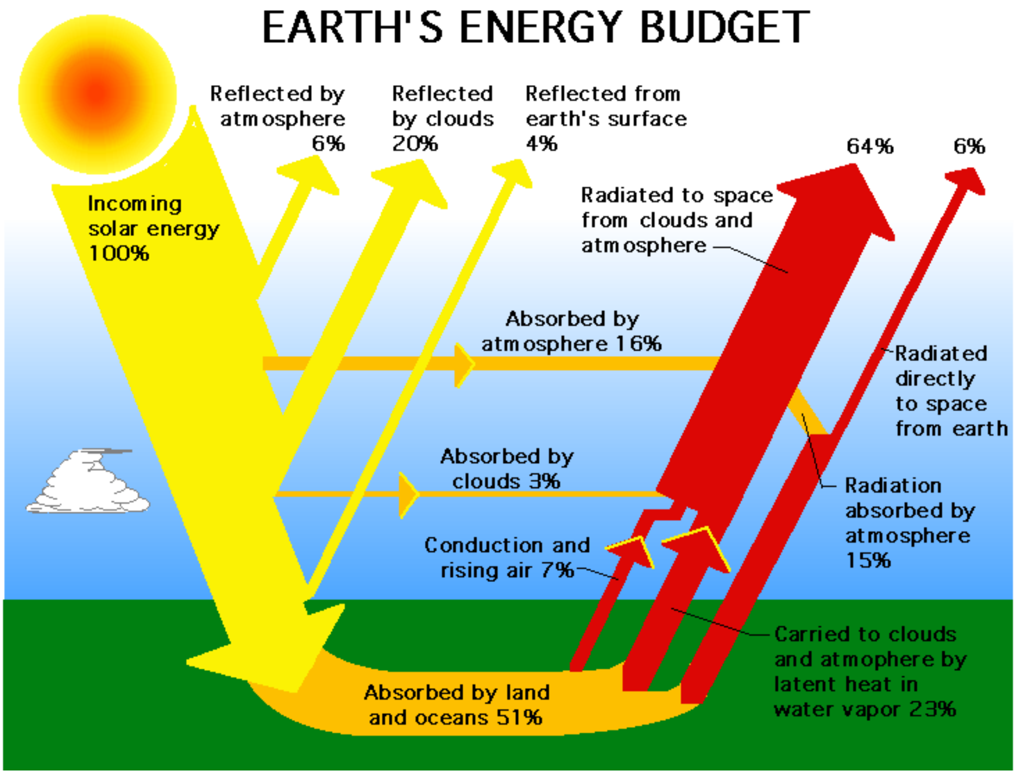

Figure 1: Energy budget of the earth/atmosphere [5]

The sun can be seen as a black body with a temperature of $T = 5500$ °C. The sun emits radiation in the shortwave region and a little bit in the long wave region. The intensity peak of the radiation is in visible wavelengths of light. The earth can also be seen as a black body, with an averaged surface and atmosphere temperature of $T = -20$ °C. The earth emits radiation in the long wave region.

Figure 2 shows the intensity and wavelength of the emitted radiation from the sun and the earth [10].

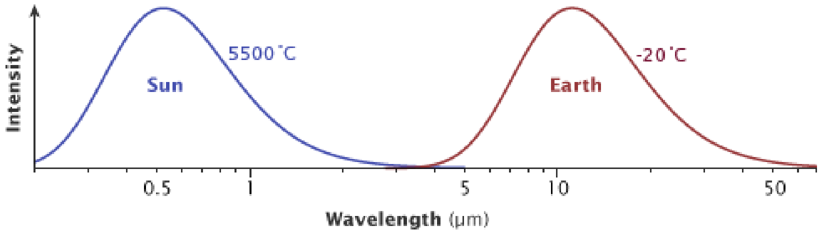

Figure 2: The intensity and wavelength of the emitted radiation from the sun and the earth; the intensity of the sun is scaled by a factor of 0.5·10^{-6} [10]

The difference between the incoming solar energy and the outgoing radiation is defined as the net radiation. The net radiation can be described as [10],

$$R_{\mathrm{n}} = SW_{\mathrm{in}} + LW_{\mathrm{in}} - SW_{\mathrm{ref}} - LW_{\mathrm{out}} \qquad (1)$$

where,

$R_{\mathrm{n}} =$	net radiation	(W/m^2)
$SW_{\mathrm{in}} =$	short wave incoming solar radiation	(W/m^2)
$LW_{\mathrm{in}} =$	long wave incoming solar radiation	(W/m^2)
$SW_{\mathrm{ref}} =$	short wave reflected solar radiation	(W/m^2)
$LW_{\mathrm{out}} =$	long wave outgoing earth radiation	(W/m^2)

The net radiation is the energy which is available for different land surface processes. The processes are the sensible heat flux (defined as conduction and heated rising air), latent heat flux and is transferred into the ground (soil heat flux). The net radiation can also been written as [1,2],

$$R_{\mathrm{n}} = H + L_{\mathrm{v}}E + G_{\mathrm{s}} \qquad (2)$$

where,

$H =$	sensible heat flux	(W/m^2)
$L_{\mathrm{v}}E =$	latent heat flux	(W/m^2)
$G_{\mathrm{s}} =$	soil heat flux	(W/m^2)

If the net radiation, the soil heat flux and the sensible heat flux are measured, the latent heat flux can be determined. The sensible heat flux can be measured with a scintillometer. In dry areas the sensible heat flux and the soil heat flux consume most of the available energy. In wet areas the latent heat flux is dominant [1,2].

2.2 Heat fluxes

Close to the earth surface the air is turbulent, which means that the temperature, humidity and the wind speed vary by location and time. This lower part of the atmosphere is defined as the boundary layer. After the sun rises in the morning, the solar radiation heats up the earth surface. The earth's surface heats the air, which results in a higher air temperature at the surface of the earth than at higher altitudes. This results in unstable conditions driven by buoyancy, in which heated air rises up to higher altitudes, in the form of turbulent eddies.

The turbulent boundary layer can grow to a thickness of 1 or 2 km over the day, but at night it will sink again as it cools. There is no buoyancy driven turbulence at night, so the boundary layer is stable. Eddies are produced on a scale of up to hundreds of meters, but break down into smaller and smaller eddies until they dissipate away at the millimetre scale. Eddies are turbulent vortices with a different temperature, pressure and humidity to the bulk average of the air.

The refractive index of the air is a function of the temperature and in a lesser degree of the humidity and the density of the air. If the eddies transport both heat and water vapour, their refractive index are different from their surroundings. This results in refractive index fluctuations [1,2].

2.3 The scintillation method

Electromagnetic radiation through the atmosphere is distorted by a couple of processes that influence its characteristics. For example, its intensity, polarization and its phase. Two of these processes are absorption and scattering of the radiation. The most important process that influences the propagation of the electromagnetic radiation are small fluctuations in the refractive index of the air. These turbulent fluctuations in the refractive index of the air lead to intensity fluctuations in the signal, known as scintillations. An example of distortion of the wave propagation that can be seen by the eye, are distortion of the view far away seen above a hot surface, or twinkling stars seen at night.

A Large Aperture Scintillometer (LAS) and an eXtra Large Aperture Scintillometer (XLAS) consists of a transmitter and a receiver. The transmitter emits a beam of electromagnetic radiation at a near infrared wavelength and the receiver registers the beam intensity. The receiver measures the intensity fluctuations of the signal. Figure 3 shows the schematic drawing of the LAS set-up, which shows the transmitter and the receiver, the height of the beam (z), the path length between the transmitter and receiver (L), the effective aperture diameter of the XLAS (D) and the different eddy sizes bounded by l_0 and L_0, the inner and outer scale of turbulence respectively.

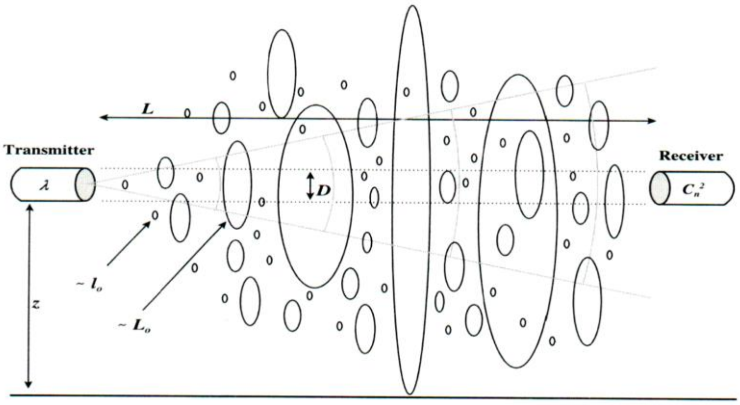

Figure 3: Schematic drawing of the LAS set-up [1]

The scintillations seen by a scintillometer can be expressed as the structure parameter of the refractive index (C_{n}^2). This parameter can be related to the transport of sensible heat and water vapour by eddies. Eddies can be seen as bubbles of air acting like positive or negative lenses.
The aperture of the transmitter and the receiver are the same, therefore the relationship between the structure parameter of the refractive index and the variation in the intensity fluctuations of the signal can be written as [1,2],

$$C_{\mathrm{n}}^2 = 1.12\sigma_{\ln I}^2 D^{\frac{7}{3}} L^{-3} \tag{3}$$

where,

$C_{\mathrm{n}}^2 =$	structure parameter of the refractive index of air	($\mathrm{m}^{-2/3}$)
$\sigma_{\ln I} =$	variance of the logarithm of intensity fluctuations	(-)
$D =$	effective aperture diameter of the XLAS	(m)
$L =$	path length	(m)

The scintillometer is most sensitive to eddies half way between the transmitter and the receiver than eddies near to them. Figure 4 shows the path weight as a function of the relative position u, which is defined as,

$$u = \frac{x}{L} \tag{4}$$

where,

$u =$	normalized position	(-)
$x =$	distance from the transmitter	(m)

From Figure 4 can be concluded that the scintillometer is most sensitive in the centre of its path and not sensitive at the transmitter and receiver.

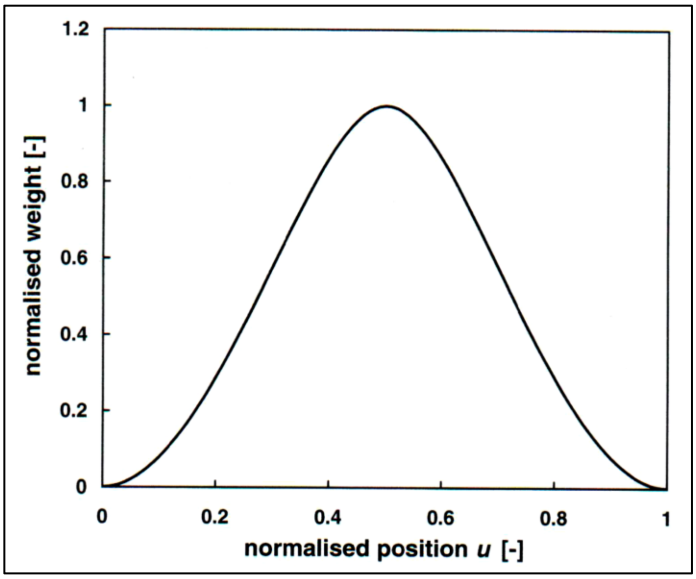

Figure 4: The path weight as function of the relative position [1]

2.4 The transmitted signal

The relative contribution of the temperature and the humidity fluctuations to the refractive index fluctuations are wavelength dependent. The temperature fluctuations are dominant at visible and near infrared wavelengths. If the wavelength increases up to several meters, the contribution of the humidity fluctuations increases. The wavelength of the emitted beam from the LAS transmitter is equal to $\lambda = 850\ \mathrm{nm}$. So the contribution of the temperature fluctuations to the refractive index fluctuations are dominant. This wavelength is chosen because at this wavelength the radiation is invisible and is less absorbed by the atmosphere. If a wavelength was chosen where the radiation is strongly absorbed by the atmosphere, there would be little or no signal detected by the receiver. The light is emitted by a single light emitting diode (LED).

It is important that the receiver only measures the signal from the transmitter, and not the radiation from the sun or other interfacing sources. To prevent this, the light emitted by the transmitter is pulsed by a LED with a frequency of 7 kHz. As an extra measure to reduce unwanted external light, the light is filtered by an absorption filter with a wavelength of $\lambda = 850$ nm and a bandwidth of 40 nm. Figure 5 shows above the transmitted signal and below an example of a received signal.

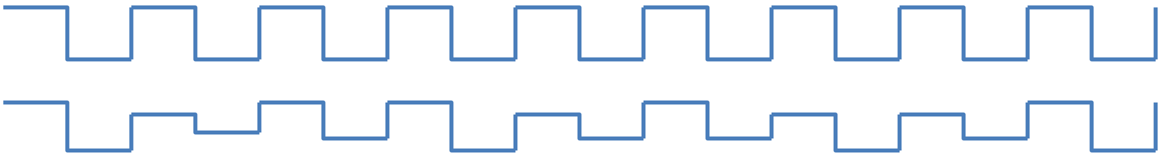

Figure 5: Above the transmitted signal and below an example of a received signal

Thereafter the signal is amplified two times with a factor of 1000, and thereafter filtered with a low pass filter of 7 kHz. After the filter the signal has positive and negative components, but by demodulating the signal, the signal becomes positive. The signal is filtered with a low pass filter of 400 Hz, because the relevant data i.e. the scintillation frequency spectrum, has a frequency below 400 Hz. The signal is also filtered with a high pass filter of 0.5 Hz. Figure 6 shows the demodulated signal with the averaged voltage.

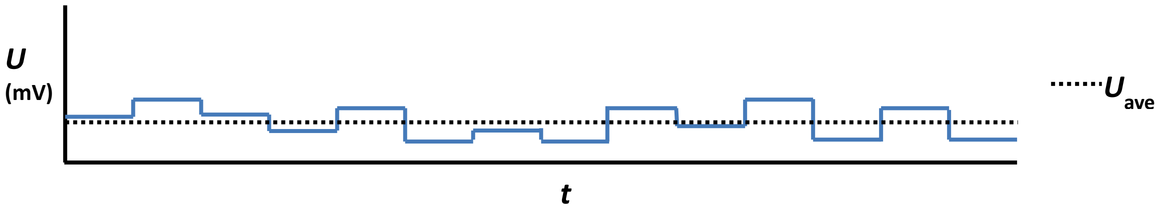

Figure 6: An example of the demodulated signal with the voltage as function of the time

The variance of intensity fluctuations is equal to a factor of the variance in the signal and the averaged voltage. The variance of intensity fluctuations can be written as,

$$\sigma_{\ln I} = \frac{U_{\mathrm{var}}^2}{U_{\mathrm{ave}}^2} \qquad (5)$$

where,

$U_{\mathrm{var}} =$	Variance in the amplitude with a sample frequency of 800 Hz	(mV)
$U_{\mathrm{ave}} =$	Averaged voltage over 5 s	(mV)

2.5 Saturation

When the turbulence becomes to intensive, the relation between the structure parameter of the refractive index and the variance of the intensity fluctuations will fail. This phenomenon is defined as saturation of the signal. Saturation occurs when the variance in the intensity fluctuations becomes higher than 0.3. When this happens an increase in the turbulence does not result in an increase of the variance of intensity fluctuations. The effect of saturation can be explained with Figure 7, which shows a wave front which propagates through a strong scattering medium and thereafter propagates through eddy *F*. Eddy *F* can be seen as a lens. When a wave front propagates through a strong scattering medium, the eddies scatter the wave front which results in small irregularities in the wave front. When the size of the irregularities are smaller than the size of *F*, then the power of lens *F* will decrease. This will lead to a pattern shown in Figure 7 at $x = L$, which is different in size and format in comparison with a single eddy and an undisturbed wave front. If the irregularities in the wave front are bigger than *F*, then the pattern at $x = L$ will not change in size but only in position.

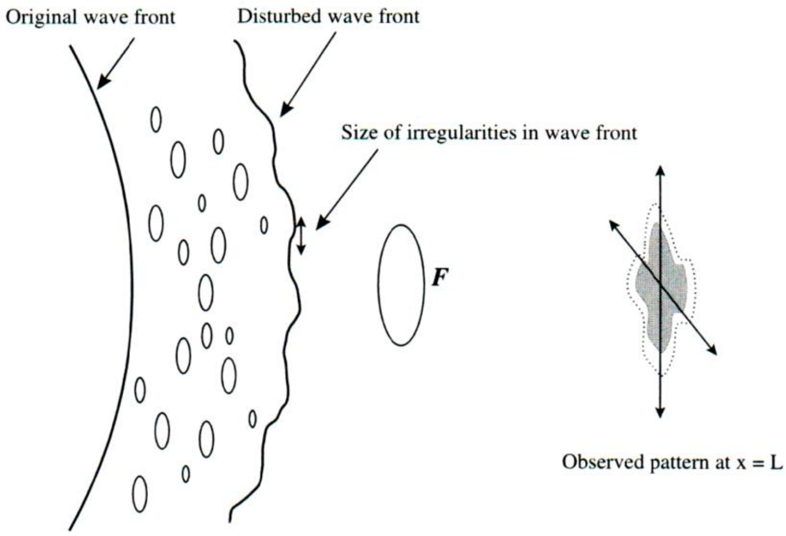

Figure 7: Irregularities by strong turbulent conditions [1]

Saturation can be avoided by limiting the path length or increasing the aperture of the scintillometer. A very small aperture scintillometer is more sensitive to smaller scales in the scintillation pattern. When the aperture of the scintillometer increases, the scintillometer will average out the small structures. This results in a decrease of the variance in the intensity fluctuations. Very large structures larger than the aperture of the scintillometer do not produce intensity fluctuations in the signal. Structures of the same size of the aperture of the scintillometer are dominant [1].

2.6 Sensible heat flux

Fluctuations in the temperature, humidity and to a lesser extent pressure cause fluctuations of the refractive index of air. Therefore the structure parameter of the refractive index can be written as a function of the structure parameter of the temperature, humidity and the covariant term as follows [1,2],

$$C_{\mathrm{n}}^{2}=\frac{A_{\mathrm{T}}^{2}}{T^{2}}C_{\mathrm{T}}^{2}+\frac{2A_{\mathrm{T}}A_{\mathrm{Q}}}{TQ}C_{\mathrm{TQ}}+\frac{A_{\mathrm{Q}}^{2}}{Q^{2}}C_{\mathrm{Q}}^{2} \quad (6)$$

where,

$A_{\mathrm{T}} =$	constant of temperature	(-)
$A_{\mathrm{Q}} =$	constant of humidity	(-)
$T =$	temperature	(K)
$Q =$	absolute humidity	(kg/m^3)
$C_T =$	structure parameter of temperature	(Km$^{-2/6}$)
$C_Q =$	structure parameter of humidity	(kgm^{-3}m$^{-2/6}$)
$C_{TQ} =$	structure parameter of humidity and temperature	(Kkgm^{-3}m$^{-2/3}$)

The constant of temperature and humidity are functions of the wavelength and the mean values of the temperature, absolute humidity and pressure. These constants represents the relative contribution of each term to the structure parameter of refractive index. In the near infrared spectrum the constant of temperature is defined as [1,2],

$$A_{\mathrm{T}}=-m_{1}\left(\frac{P}{T}\right)-m_{2}R_{\mathrm{V}}Q \quad (7)$$

where,

$P =$	pressure	(Pa)
$R_{\mathrm{V}} =$	specific gas constant for water vapour	(461.5 J/kgK)
$m_1 =$	wavelength dependent constant, $0.780\cdot 10^{-6}$	(K/Pa)
$m_2 =$	wavelength dependent constant, $-0.126\cdot 10^{-6}$	(K/Pa)

and the constant of humidity is defined as [1,2],

$$A_{\mathrm{Q}}=m_{2}R_{\mathrm{V}}Q \quad (8)$$

The constant of temperature is much bigger than the constant of humidity, so for the wavelength in the near infrared the temperature fluctuations are dominant. Because the constant of temperature is much bigger than the constant of humidity, the structure parameter of the refractive index can be defined as [1,2],

$$C_{\mathrm{n}}^{2}\approx\frac{A_{\mathrm{T}}^{2}}{T^{2}}C_{\mathrm{T}}^{2}\left(1+\frac{0.030}{\beta}\right)^{2} \quad (9)$$

where,

$\beta =$ Bowen ratio (-)

The Bowen ratio is defined as the ratio between the sensible heat flux and the latent heat flux, therefore the Bowen ratio can be written as [1,2],

$$\beta = \frac{H}{L_{\mathrm{V}} E} \tag{10}$$

When formula 7 and 9 are combined, the structure parameter of the refractive index can be written as [1,2],

$$C_{\mathrm{n}}^2 \approx \left(\frac{-m_1 P}{T^2}\right)^2 C_T^2 \left(1 + \frac{0.030}{\beta}\right)^2 \tag{11}$$

In dry areas the sensible heat flux is larger than the latent heat flux, which results in a Bowen ratio of three or bigger. In wet areas the Bowen ratio is smaller than 0.5, therefore the influence of the humidity fluctuations is higher which results in a large correction. In the Netherlands the Bowen ratio is equal to $\beta = 2$.The structure parameter of the temperature can be calculated from formula 11. Therefore the structure parameter of the temperature can been written as [1,2],

$$C_{\mathrm{T}}^2 \approx C_{\mathrm{n}}^2 \left(\frac{-m_1 P}{T^2}\right)^{-2} \left(1 + \frac{0.030}{\beta}\right)^{-2} \tag{12}$$

When the atmosphere is unstable and the XLAS is mounted high above the surface (≈20 m) the sensible heat flux from the free convection method can be written as [1,2],

$$H_{\mathrm{free}} = b \rho c_{\mathrm{p}} (z - d) \left(\frac{g}{T}\right)^{1/2} (C_{\mathrm{T}}^2)^{3/4} \tag{13}$$

where,

$H_{\mathrm{free}} =$	sensible heat flux from free convection method	(W/m^2)
$b =$	free convection limit, 0.48	(-)
$\rho =$	density of air	(kg/m^3)
$c_{\mathrm{p}} =$	heat capacity of air	(1005 J/kgK)
$d =$	zero displacement height	(m)
$g =$	gravitational acceleration	(m/s^2)

3 eXtra Large Aperture Scintillometer

In this chapter the components of the XLAS are described. The focal length of the Fresnel lens is determined in order to transmit a parallel bundle and receive the maximum signal. Than the measurement set-up and the working method are explained.

3.1 Main components of the XLAS

The XLAS consists of a transmitter, which emits a collimated or parallel light beam and a receiver which detects the signal. Figure 8 shows the XLAS. The light beam is emitted by a LED with a wavelength of $\lambda = 850$ nm. The LED is mounted on a translation stage with a motion of range of 20 mm. The translation stage is mounted on the LED back plate. The LED can be placed 20 to 40 mm from the LED back plate. The LED back plate is mounted on a ring, which is fixed within the end of the small tube. Figure 9 shows a cross-section of the XLAS transmitter. Number 1 is the LED and number 2 is the small tube.

Figure 8: View of the XLAS

A detector is used to convert the received signal into a voltage. The detector is placed on the LED back plate in the receiver. A band pass filter is placed in front of the detector, to detect only wavelengths in the range of the transmitted wavelength, and block strong light. The filter has a centre wavelength of 850 nm and a full width at half maximum of 40 nm [11].

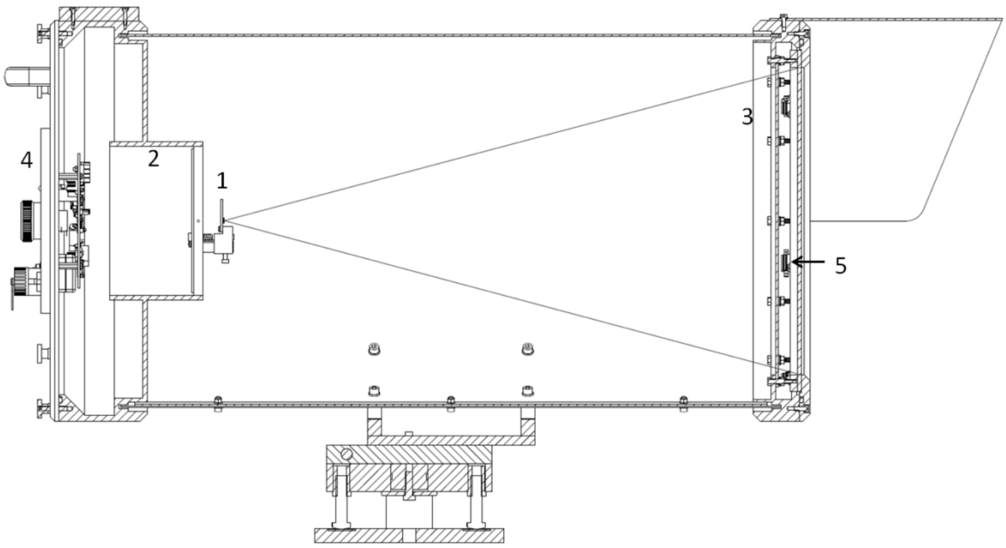

Figure 9: A cross-section of the XLAS transmitter

A Fresnel lens is used to propagate the beam parallel through the medium and to focus the beam on the detector. The Fresnel lens is labelled number 3 in Figure 9. Fresnel lenses consists of a series of grooves in a circle. When the grooves have the same form as a spherical lens, as shown in Figure 10, then the focal length of both lenses are the same. The advantage of the Fresnel lens in comparison with a spherical lens is less space, less weight and less absorption. The disadvantage of the Fresnel lens is the light is distorted by the grooves edges, so it is not so well suited for imaging applications, but good at light gathering applications. At higher groove intensity the distortion will decrease, but transmission will decrease.

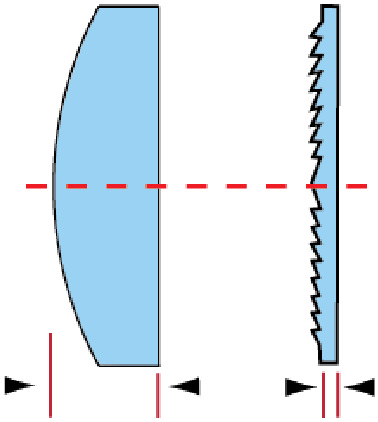

Figure 10: Left the sphere lens and right the Fresnel lens [6]

The aperture of the Fresnel lens used for the XLAS is $D = 328$ mm. The focal length of the lens is $f = 610 \pm 30$ mm. The refractive index of an acrylic ($C_5O_2H_8$) lens is $n = 1{,}49$ [7].
To avoid condensation on the window, a heating ring is placed behind the window. The heating ring is labelled number 5 in Figure 9. The heating ring consists of an aluminium ring with 6 resistors [12]. The Fresnel lens is placed behind the heater ring.

The back panel of the XLAS receiver consists of a power supply input, a digital input/output, analogue output, sensor input and a keyboard with a display. The XLAS transmitter consists of a LED driver and output power adjustment, which is labelled number 4 in Figure 9. The display can show the received signal, structure parameter of the refractive index. Configuration settings of the XLAS can be changed using the keyboard. The sensor input has a 12 VDC power supply for the sensors and needs a 4 to 20 mA output from the sensors. The digital serial gives the date and time, the output voltage, the variance of intensity fluctuations, the structure parameter of the refractive index and the calculated sensible heat flux from the temperature, pressure and wind speed for each time interval. The analogue output gives the output voltage and the structure parameter of the refractive index calculated from the signal level. With the analogue output the structure parameter need to be converted from 0 to 2 V to the units $m^{-2/3}$ afterwards.

A telescope is used to align the transmitter and the receiver with each other, otherwise it is difficult to find the other XLAS over a distance of 10 km.

3.2 Determining the focal length of the Fresnel lens

The focal length of the Fresnel lens is dependent on the wavelength of the light. The focal length increases when the wavelength of the light also increases. If the LED is placed in the focal length of the Fresnel lens, the light leaves the XLAS in a parallel beam. Figure 11 shows the schematic view of the transmitter of the XLAS. The LED is mounted on a translation stage, this is mounted on a panel which can be mounted on a ring in the inside of the tube. The position of the mounting ring in the tube can be changed in the initial assembly.

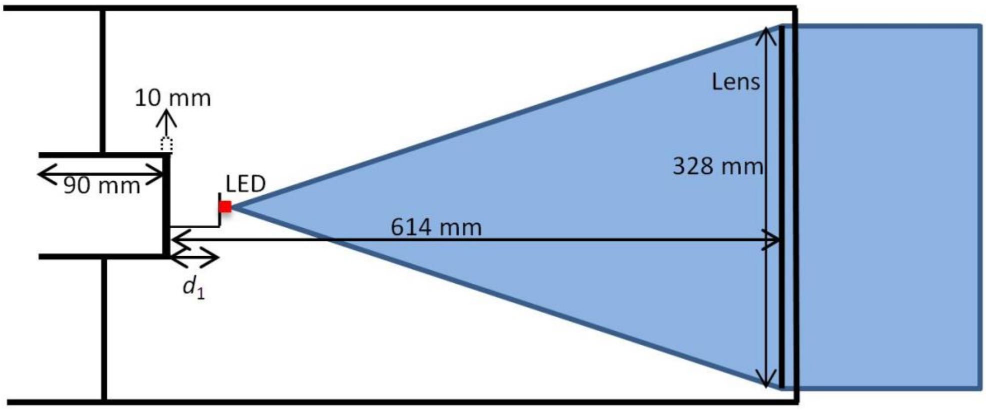

Figure 11: Schematic view of the transmitter

The translation stage of the LED has a range of motion of 20 mm, so the LED can be placed at the focus correctly. The distance from the LED to the LED back plate (d_1) is between 20 and 40 mm. The focal length of the Fresnel lens is measured in two different ways. The first method is to determine the diameter of the bundle over a distance of 15 m to check if it is parallel. When the LED is placed at the focal point, the bundle must be parallel over the entire distance of 15 m. If the bundle is parallel over the whole distance, than the LED is correctly placed in the focal position. Figure 12 shows the light beam as viewed from the XLAS.

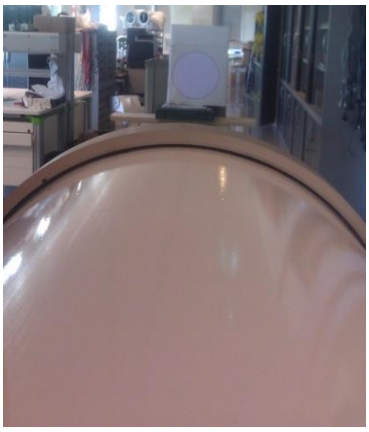

Figure 12: The blue test beam shown from the XLAS

The second method to measure the focal length of the lens is to send light with the transmitter in a parallel bundle and receive the light with the receiver over a distance of 15 m. A thin target of paper was placed on the receiver plate, over the centre hole, so the bright spot at the focus point of the lens can be seen. Figure 13 illustrates the setup of the receiver plate for the imaging of the spot.

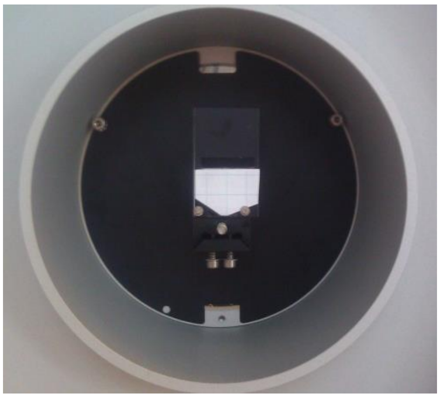

Figure 13: The paper viewing screen in the receiver plate for imaging of the focal spot

The focal length of the transmitter is determined by method one and the focal length of the receiver is determined by method two. The focal length of the lens is determined for each lens, because the deviation in the focal length can be ± 30 mm. The focal length is determined at a wavelength of $\lambda = 470$ nm, $\lambda = 537$ nm and $\lambda = 632$ nm, by using red, green and blue LED's of the same size and type as the infrared Platinium Dragon LED used for actual LAS measurements. The refractive index is different for each wavelength. The relationship between the refractive index and the wavelength is given by the Sellmeier equation, with the constants given for acrylic, written as [8,9],

$$n = \sqrt{1 + \frac{B_1}{1 - \frac{C_1}{\lambda^2}} + \frac{B_2}{1 - \frac{C_2}{\lambda^2}} + \frac{B_3}{1 - \frac{C_3}{\lambda^2}}} \qquad (14)$$

where,

$n =$	refractive index	(-)
$\lambda =$	wavelength	(nm)
$B_1 = 0.9965$		(-)
$B_2 = 0.1896$		(-)
$B_3 = 0.004110$		(-)
$C_1 = 7.870 \text{ x } 10^{-15}$		(nm^2)
$C_2 = 2.191 \text{ x } 10^{-14}$		(nm^2)
$C_3 = 3.857 \text{ x } 10^{-12}$		(nm^2)

Sample equation 4, in Appendix B: Sample equations, calculates the refractive index for a wavelength of 632 nm. Table 1 gives the refractive index as function of the wavelength determined by equation 14. The refractive index decreases if the wavelength increases.

Table 1: The refractive index as function of the wavelength

λ (nm)	*n* (-)
400.0	1.506
470.0	1.498
537.0	1.493
632.0	1.489
850.0	1.484
1000.0	1.482

The Fresnel lens can be seen as a plano convex lens, so the focal length of the lens can be written as [3],

$$f = \frac{1}{(n-1)\left(\frac{1}{R_1} - \frac{1}{R_2}\right)} \quad (15)$$

where,

$f =$	focal length	(mm)
$R_1 =$	radius of curvature of the convex side of the lens (275.5 mm)	(mm)
$R_2 =$	radius of curvature of the plano side of the lens (= ∞)	(mm)

The focal length is a function of the refractive index, so also a function of the wavelength of the light. If the wavelength increases, the refractive index decreases and the focal length increases. Sample equation 5, in Appendix B: Sample equations, calculates the focal length of the Fresnel lens for a wavelength of 632 nm. Table 2 gives the focal length as function of the wavelength determined by equation 15.

Table 2: The calculated focal length as function of the wavelength

λ (nm)	*n* (-)	*f* (mm)
400.0	1.506	544.6
470.0	1.498	553.4
537.0	1.493	558.7
632.0	1.489	563.5
850.0	1.484	569.3
1000.0	1.482	571.4

The focal length is measured by method one and two. The focal length is determined by measuring the distance between the LED and the LED back plate, determined as d_1. The focal length is equal to the distance between the lens and front ring plus the thickness of the ring minus distance d_1. Table 3 shows the measured focal length as function of the wavelength. XLAS numbers T140001 and T140002 are transmitters and R140001 and R140002 are receivers. There is a little difference between the two methods, but the difference is within the uncertainty.

Table 3: The measured focal length for the different wavelengths for the two methods

XLAS number	λ (nm)	Method 1 d_1 (mm) ± 5 mm	Method 1 f (mm) ± 5 mm	Method 2 d_1 (mm) ± 5 mm	Method 2 f (mm) ± 5 mm
T140001	470	51	573	N/A	N/A
	537	44	580	N/A	N/A
	632	40	584	N/A	N/A
R140001	470	43	581	44	580
	537	35	589	38	586
	632	30	594	31	593
T140002	470	49	575	N/A	N/A
	537	43	581	N/A	N/A
	632	37	587	N/A	N/A
R140002	470	50	574	49	575
	537	43	581	45	579
	632	39	585	41	583

Distance d_1, for a LED with a wavelength of 850 nm, can be determined by calculating the ratio between the measured and the theoretical focal length. The distance d_1 in the four scintillometers are shown in Table 4. Distance d_1 is between the 20 and 40 mm, so the calculated distances are within the range of motion of the LED, which is restricted by the opto-mechanical mount.

Table 4: The distance of the LED above the LED back plate for the four scintillometers

XLAS number	d_1 (mm) ± 5 mm
T140001	34
R140001	25
T140002	33
R140002	34

3.3 Kipp & Zonen roof setup with meteorological sensors

A calibration table is installed on the Kipp & Zonen roof to align, test and calibrate LAS instruments. A transmitter and receiver are installed on the roof of the Technical University Delft (TU) building of electronic and mathematics. The distance between the TU roof and the Kipp & Zonen roof is 889 m as measured by Google maps and by a portable GPS. The beam of the LAS spreads out slightly with distance, so over 889 m more than one receiver can detect the same transmitted signal. The transmitter on the TU roof transmits the signal to the receivers on the Kipp & Zonen roof and vice versa. Figure 14 shows a view of the calibration table on the Kipp & Zonen roof. The first level of the table consists of reference LAS R120001 and control LAS R120002, a transmitter and two mounts for additional research and development (R&D) LAS. The second level consist of XLAS receiver R140002 on position 1 and XLAS receiver R140001 on position 8 and space for six other receivers. A CR9000XC Campbell Scientific data logger was used to log the analogue data from three receivers. Six meteorological sensors were placed on and above the table, to monitor the general weather conditions.

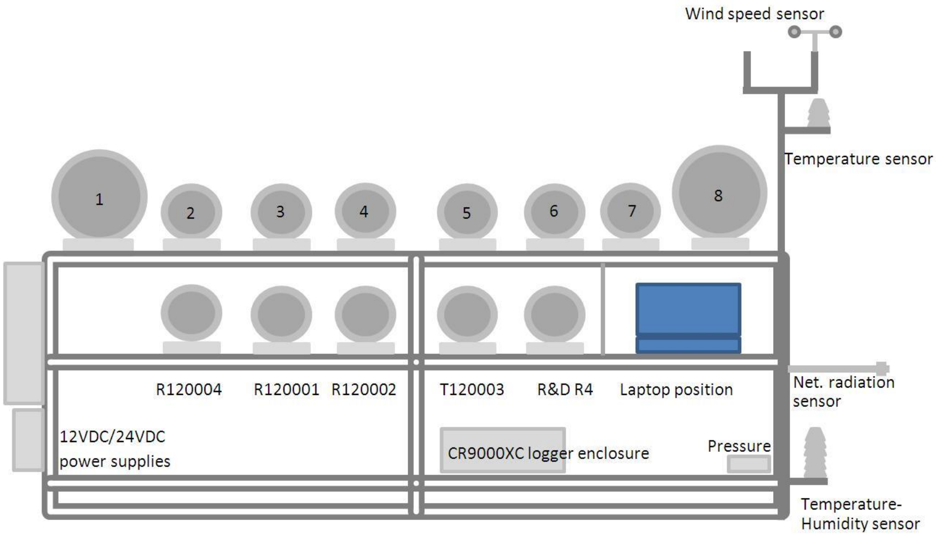

Figure 14: The calibration table of the LAS with the meteorological sensors, viewed from the rear

Meteorological instruments can measure meteorological characteristics of the air, such as temperature, pressure and humidity. Meteorological instruments can also be used to calculate the sensible heat flux, in combination with data from a LAS. The output of the sensor could be in the form of a current, voltage or a resistance measurement. For the LAS/XLAS electronics the input needs to be in the form of a current with a range from 4 to 20 mA. In the LAS data logger configuration set up the corresponding actual value from the instrument at 4 and 20 mA need to be given. So for example for the temperature sensor, 4 mA corresponds to a temperature of -40 ^{o}C and 20 mA corresponds to + 60 ^{o}C. The meteorological sensors which were used are a temperature sensor at 2.5 m, pressure sensor, wind speed sensor, temperature and humidity sensor (at 0.5 m) and a net radiation sensor.

The temperature, pressure and wind speed were used to calculate the sensible heat flux in combination with data from the reference scintillometer R120001. The sensors were connected to an interface box, which connects the power supplies to the sensors and connects the output of three sensors into one signal cable to the LAS. The temperature-, wind speed- and pressure sensors were connected to LAS 120001. The temperature and humidity sensor and the net radiation sensor were connected to LAS 120002. Figure 15 shows the connection of the sensors to the sensor box and the LAS.

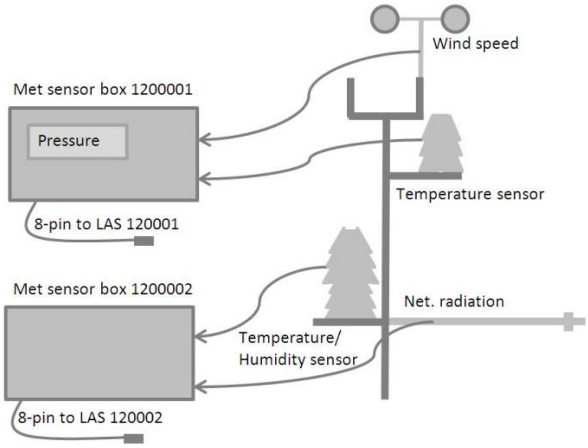

Figure 15: View of the meteorological sensors connected to a sensor box and the LAS.

Table 5 gives the description, the installation height, analogue output, measuring range, sensitivity and uncertainty of the meteorological sensors connected to LAS 120001. Table 6 shows the characteristics of the met sensors connected to LAS 120002.

Table 5: Characteristics of the meteorological sensors connected to LAS 120001

Met sensor	Description	Analogue output	Measuring range	Sensitivity	Uncertainty
Air temperature	Merij Meteo MT42, Kipp no. 650020008, installation height: 50 cm	4…20 mA	-40…+60 °C	0.1600 mA/°C	± 0.1 °C
Air pressure	Theodor Friedrichs, 5004.2000, installation height: 65 cm	4…20 mA	900…1050 hPa	0.1067 mA/hPa	± 1 hPa
Wind speed	Merij Meteo MW 35, installation height:290 cm	4…20 mA	0…40 m/s	0.4000 mA/(m/s)	± 0.6 m/s

Table 6: Characteristics of the meteorological sensors connected to LAS 120002

Met sensor	Description	Analogue output	Measuring range	Sensitivity	Uncertainty
Air temperature	Theodoric Friedrichs, 3032.0200, humidity and temperature sensor, installation height: 250 cm	4…20 mA	-35…+45 °C	0.2000 mA/°C	± 0.2 °C
Air humidity		4…20 mA	0…100%	0.1600 mA/%	± 2 %
Net radiation	Kipp & Zonen, NR2 lite C36.2, installation height: 74 cm	4…20 mA	-400…1200 W/m^2	0.0100 mA/(W/m^2)	± 20 W/m^2

3.4 Working method

In this paragraph the working method of the experiments are explained. First the frequency spectrum of the scintillometer is explained. Thereafter the comparison between the XLAS and the LAS, the LAS and the Wageningen LAS, and the LAS and the Scintec LAS are explained.

3.4.1 Working method for measuring frequency spectrum scintillometers

The scintillometer measures a typical scintillation spectrum. The frequency spectrum is investigated to see if the scintillometers are responding to this typical scintillation spectrum. A Campbell Scientific CR9000XC data logger is used to sample the raw demodulated signal from the LAS at 500 Hz (along with the filtered C_{n}^2 data at a lower frequency). The frequency spectrum displayed are unfiltered, but normally in the LAS the data is internally filtered between 0.53 and 400Hz. Therefore normally frequencies lower than 0.53 Hz (corresponding to changing atmospheric absorption) and higher than 400 Hz (electrical noise) will be filtered from the raw signal. From 16 May the high pass filter setting in LAS receiver 040007 was changed to 0.1 Hz, to avoid loss of C_{n}^2 at low wind speed and allow comparison of a LAS with different settings.
The scintec LAS does not store the raw data, so the frequency spectrum of the scintec LAS cannot be shown.

3.4.2 Working method for comparison between XLAS and LAS

The XLAS was compared with the LAS to investigate if the scintillometers measure the same eddies. The XLAS was compared with reference LAS 120001, LAS 120001 was checked with the control LAS 120002. The XLAS and the LAS are most sensitive for eddies of the size of the diameter of the aperture. Therefore the LAS responds more strongly to smaller eddies than the XLAS. A reduction ring was placed in front of the window of the XLAS. The reduction ring has the same aperture diameter as the aperture of the LAS. When the ring was placed the LAS and the XLAS should respond in the same way and measure the same scale of eddies, namely 150 mm. Window elements in the LAS can reduce the effective diameter of the LAS, so the effective diameter would be 149 mm.
The LAS transmitter on the TU roof transmits the signal and LAS 120001, LAS 120002, XLAS 140001 and XLAS 140002 receive the signal on the roof of Kipp & Zonen. The comparison was started at 1 April and ended on 25 May. In this period a few ideal or representative days are chosen to do the comparison between the XLAS and the LAS.

3.4.3 Working method for comparison between LAS and WagLAS

The precursor for the LAS was based on a prototype developed by the University of Wageningen. Therefore the LAS is compared with the Wageningen LAS to investigate if the scintillometers respond equally well and give the same or similar absolute values. The Wageningen LAS has a round parabolic mirror which reflects and focuses the received signal on to the detector. The diameter of the aperture is around the same as the aperture of the LAS from Kipp & Zonen, namely 149 mm.
The transmitter of the Wageningen LAS was placed on position 3 on the table on the roof of Kipp & Zonen. The Wageningen receiver was placed on the TU roof. The transmitter of Kipp & Zonen was placed on the TU roof and the LAS receivers 120001 and 120002 were placed on the table on the roof of Kipp & Zonen. Therefore the paths of the 2 sets of instruments were reversed, but are measuring equivalent columns of air.

The comparison was started on 16 April and ended on 16 May. In this period a few ideal or representative days are chosen to compare the data between the LAS and the Wageningen LAS.

3.4.4 Working method for comparison between LAS and scintec LAS

The LAS was compared with a LAS from Scintec, the BLS900, which is a competitor of Kipp & Zonen for LAS. The BLS900 consists of two transmitter disks. Each disk has 444 infrared LED's and 18 red LED's. The BLS900 can operate in four different pulse modes to save power. The signal on disk one is transmitted at a frequency of 1750 Hz and on disk two is transmitted at a frequency of 2500 Hz. The transmitter LED array emits light over an angle of 16 degrees. The aperture diameter is 140 mm [13].

The BLS900 transmitter was placed on position 4 on the table on the roof of Kipp & Zonen. The BLS900 receiver was placed on the TU roof. The transmitter of Kipp & Zonen was placed on the TU roof and the LAS receivers 120001 and 120002 were placed on the table on the roof of Kipp & Zonen. Therefore the paths of the 2 sets of instruments are reversed, but are measuring equivalent columns of air. The comparison was started on 16 May and ended on 23 May. In this period a few ideal or representative days are chosen to compare the data between the LAS and the Wageningen LAS.

4 XLAS experiments

In this chapter the experiments with the XLAS and the LAS are described. In the first paragraph the frequency spectrum of the scintillometers are shown. In the second paragraph the comparison between the XLAS and the LAS is described and in the third paragraph the comparison between the LAS and the Wageningen LAS is described. The fourth paragraph describes the comparison between the LAS and the Scintec LAS.

4.1 Frequency spectrum scintillometers

The frequency spectrum was investigated to see if the scintillometers are responding to the typical scintillation spectrum. Figure 16 shows the frequency spectrum of XLAS 140001. This frequency spectrum corresponds with the typical frequency spectrum, in the correct range and with no interfering sources such as electrical noise or vibrations.

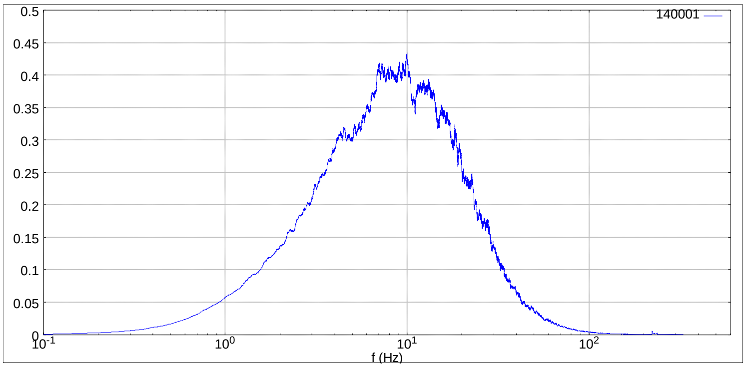

Figure 16: The intensity as function of the frequency of XLAS 140001 at 16 May 9:45

Figure 17 shows the frequency spectrum of XLAS 140002. The spectrum has the same pattern as the spectrum of 140001, but the intensity of the frequency is lower than the frequency spectrum of XLAS 140001.

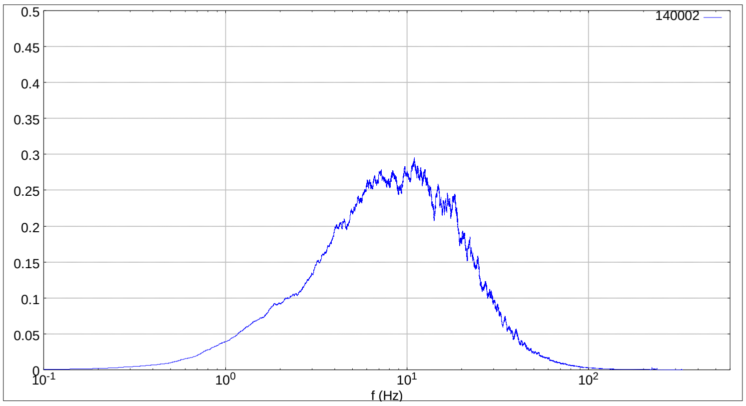

Figure 17: The intensity as function of the frequency of XLAS 140002 16 May 9:45

Figure 18 shows on the left the frequency spectrum of LAS 120001. The spectrum is shifted to the right in comparison with the spectrum of the XLAS. This can be a result of a larger crosswind, because the frequency spectrum is measured at a different time period, one hour later than for the XLAS. Figure 18 shows on the right the frequency spectrum of LAS 120002. The frequency spectrum has the same pattern as the spectrum of LAS 120001.

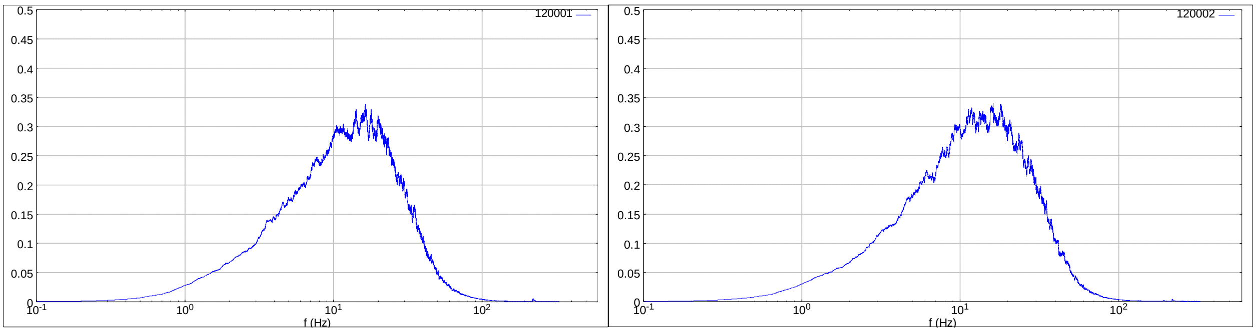

Figure 18: Left the intensity as function of the frequency for LAS 120001 at 16 May 10:45 and right The intensity as function of the frequency for LAS 120002 at 16 May 10:45

Figure 19 shows the frequency spectrum of the Wageningen LAS. The spectrum has the same pattern as the LAS and the XLAS, but has a high spike around 155 Hz and some small spikes around 33 and 35 Hz. This detector is optimised for using the LAS at long path lengths, i.e. high gain, but that means it is noisier than the regular detector (the detector can be swapped out for different experiments).

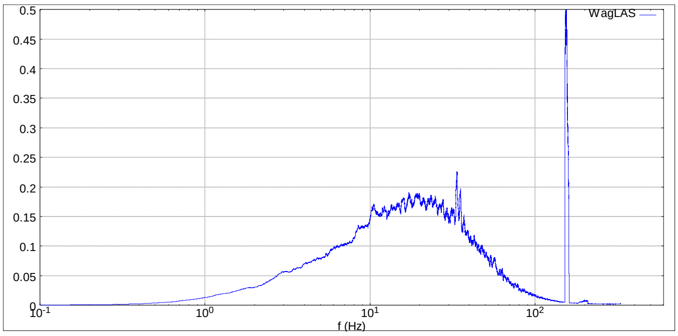

Figure 19: The intensity as function of the frequency for the Wageningen LAS at 15 May 10:00

Figure 20 shows the frequency spectrum of LAS 040007. The spectrum has the same pattern as the spectrum of the XLAS and the LAS.

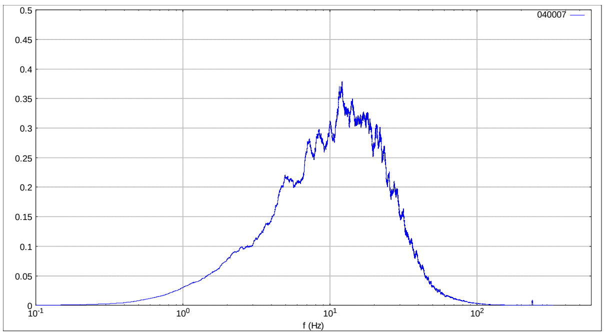

Figure 20: The intensity as function of the frequency for LAS 040007 at 16 May 11:30

4.2 Comparison between XLAS and LAS

The XLAS was compared with the LAS with a reduction ring in front of the window of the XLAS. On a clear sunny day the received signal on the LAS is around 600 to 700 mV. When it is raining or there is fog/high humidity the received signal on the LAS is below 500 mV, as light is absorbed and scattered by the water. The rain and fog can lead to a variance in the received signal which is not an influence of the heat flux, so the error in the measurement increases. Due to the rain and fog the different scintillometers could measure different variance in the received signal, and the signal to noise ratio will be worse. Therefore, when the received signal from the LAS is lower than 500 mV, the data is removed from the comparison.

The data which is used for the comparison is from 15 May to 19 May. On these four days it did not rain and the sun was shining. The days for the comparison are chosen from the data from the meteorological instruments. The meteorological data is shown in Appendix D: Meteorological data 15 – 20 May, where Figure 38 shows the temperature, Figure 39 shows the pressure, Figure 40 shows the wind speed and Figure 41 shows the net radiation. The humidity sensor was damaged during this period, so the humidity values are not shown. The net radiation is negative during the night and positive during the daytime. During clear blue skies the net radiation is higher than when there are clouds present. From the net radiation measurement it can be concluded that the first and the last day in this period were a little bit cloudy. The temperature during this period increases every day by 2 ^{o}C.

Figure 21 shows the received signal as function of the time from 15 May to 19 May. Each data point is an average of 10 minutes. The received signal on 120001, 120002 and 140002 are nearly the same, but the signal of 140001 is higher than the others. The variance in the signal is the same for all the LAS. Around 18:00 UTC time, 20:00 local Dutch time, the sun is shining directly onto the detector of the LAS, due to the orientation of the setup. This leads to an erroneous peak in the data and disturbs the data, so these periods are deleted from the data.

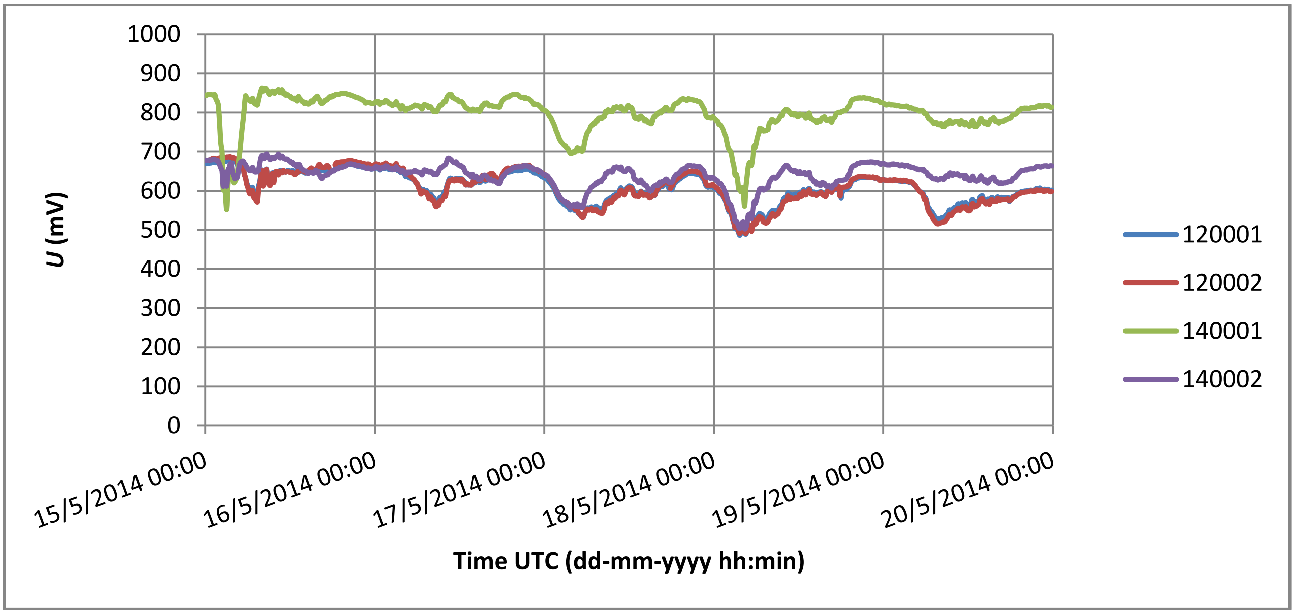

Figure 21: The received signal as function of time from 13 April to 16 April for LAS 120001 and 120002 and for XLAS 140001 and 140002

Figure 22 shows the variance of the logarithm of intensity fluctuations as function of the time. The variance is calculated by the natural logarithm of the variance in the received signal with the use of formula 5. The LAS calculates the variance every second and averages it for every 10 minutes.

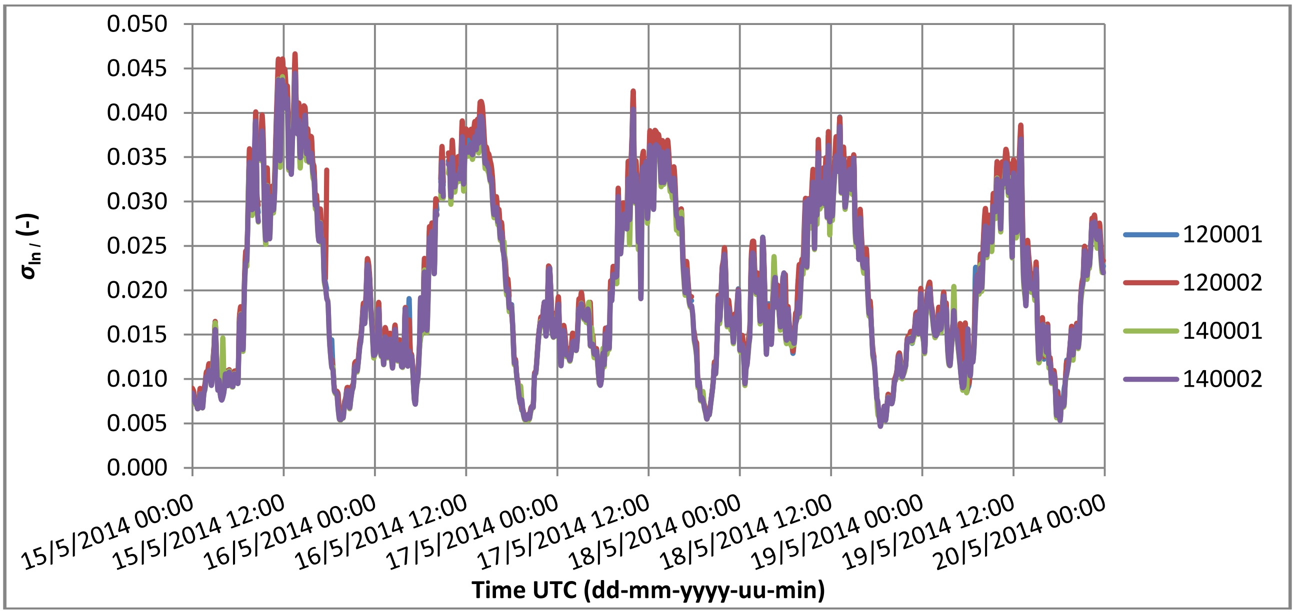

Figure 22: Variance of the logarithm of intensity fluctuations as function of time

The data from the scintillometers is compared in the form of the structure parameter of the refractive index. The parameter is calculated by the LAS itself with formula 3. Sample equation 1 calculates the structure parameter of the refractive index and is performed for LAS 120001 at 18 May 8:00,

$$C_{\mathrm{n}}^{2} = 1.12\sigma_{\ln I}^{2} D^{\frac{7}{3}} L^{-3} \qquad (3)$$

where,

$\sigma_{\ln I} = 0.0206$
$D = 0.149 \text{ m}$
$L = 889 \text{ m}$

so that,

$C_{\mathrm{n}}^{2} = 7.98 \text{ x } 10^{-15} \text{ m}^{-2/3}$

18 May 8:00 is chosen because it is the mean value of the variance in the logarithm of the intensity fluctuations. This is a representative value for further calculations.

The uncertainty is equal to the standard deviation, three times sigma. The uncertainty in the variance of the logarithm of intensity fluctuations is determined from the LINEST function in Excel over a time period of 10 minutes with a frequency of 1 Hz. The uncertainty of the structure parameter of the refractive index, calculated with LAS 120001 on 18 May 8:00, is equal to,

$$C_{\mathrm{n}}^2 = e\sigma_{\ln I}^2 D^{\frac{7}{3}} L^{-3} \tag{3}$$

$$\Delta C_{\mathrm{n}}^2 = \frac{\Delta e}{e} C_{\mathrm{n}}^2 + \frac{\Delta \sigma_{\ln I}}{\sigma_{\ln I}} C_{\mathrm{n}}^2 + \frac{\Delta D}{D} C_{\mathrm{n}}^2 + \frac{\Delta L}{L} C_{\mathrm{n}}^2$$

$$\Delta C_{\mathrm{n}}^2 = 3.57 \text{ x } 10^{-17} + 3.81 \text{ x } 10^{-16} + 5.4 \text{ x } 10^{-17} + 9.00 \text{ x } 10^{-18}$$

where,

$e = 1.12 \pm 0.005$
$\sigma_{\ln I} = 0.021 \pm 0.001$
$D = 0.149 \pm 0.001 \text{ m}$
$L = 889 \pm 1 \text{ m}$

so that,
$\Delta C_{\mathrm{n}}^2 = 5 \text{ x } 10^{-16} \text{ m}^{-2/3}$

So the structure parameter of the refractive index with uncertainty is equal to,
$C_{\mathrm{n}}^2 = (8.0 \pm 0.5) \text{ x } 10^{-15} \text{ m}^{-2/3}$

The uncertainty in C_{n}^2 for one point is equal to ± 6 % of the value. Figure 23 shows the structure parameter of the refractive index as function of the time from 15 May to 19 May. The parameter drops around sunrise and sunset. After sunrise the parameter rises to the order of 10^{-13} and just before sunset it decreases to between 10^{-15} and 10^{-16}. At night the parameter stays more stable.

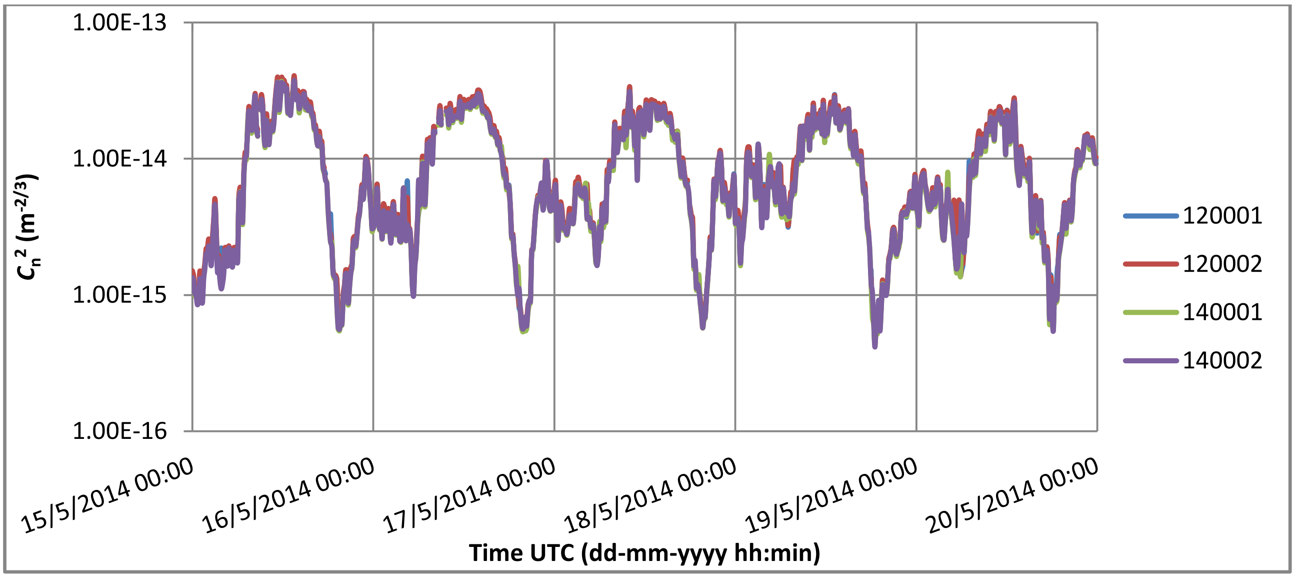

Figure 23: The structure parameter of the refractive index as function of time

To compare the results from the different receivers, the different receivers can be plotted as a function of each other. The slope of the scatterplot will be equal to one when the receivers measure the same value. Figure 24 shows the structure parameter of the refractive index of receiver 120002 as function of the structure parameter of the refractive index of receiver 120001. The slope of the scatterplot is 1.032 ± 0.005, which means that 120002 measures 3.2 ± 0.5 % higher values than 120001. The uncertainty in the slope of the scatterplot is calculated with the LINEST function in excel. The difference between the reference and the control receiver is small enough to compare LAS 120001 with the two XLAS receivers. 99.9 % of the values fit the trend line.

Table 8, in Appendix E: Results comparison 1 April – 25 May, shows the slope and the R^2 of the structure parameter of the refractive index for LAS 120002 as function of LAS 120001 for different time periods. Over these periods the values fit the line at least within 98.8 % and the mean of the slope is 1.028 ± 0.005. This means that LAS 120002 measures 2.8 ± 0.5 % higher values than LAS 120001 over a period of two months.

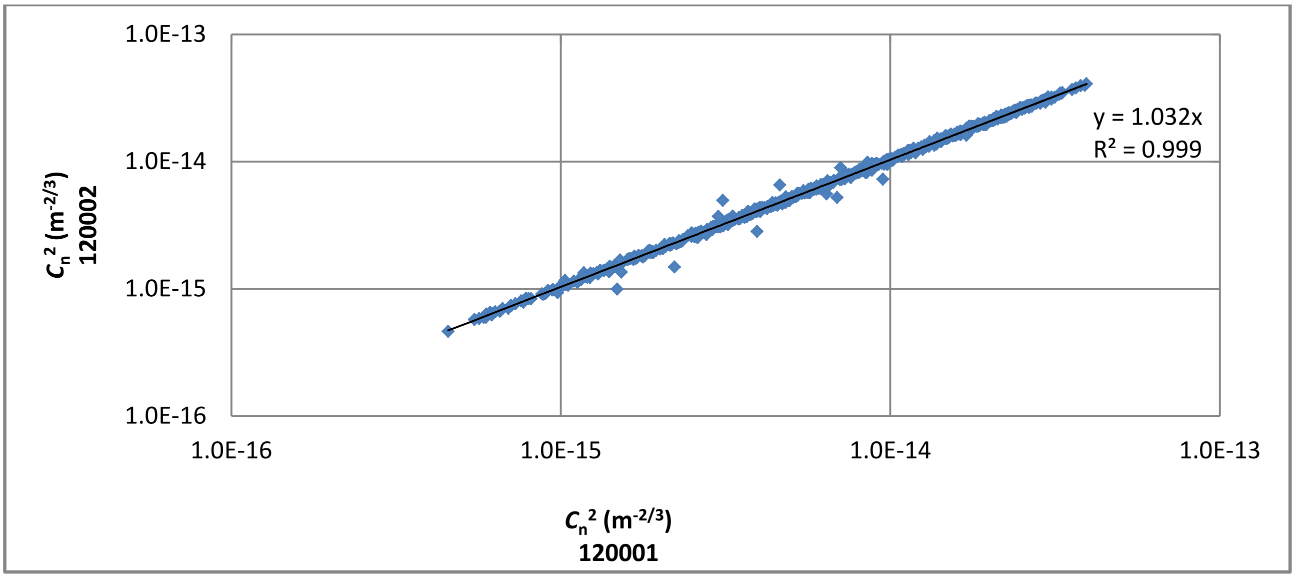

Figure 24: LAS 120002 as function of LAS 120001

Figure 25 shows on the left the structure parameter of the refractive index of XLAS 140001 as a function of the structure parameter of the refractive index of LAS 120001. The slope of the scatterplot is equal to 0.934 ± 0.007, which means that 140001 measures 6.5 % lower than the reference LAS. 99.5 % of the values fit the trend line. Figure 25 shows on the right the structure parameter of the refractive index of XLAS 140002 as function of the structure parameter of the refractive index of LAS 120001. The slope of the scatterplot is equal to 0.959 ± 0.009, which means that 140002 measures 4.2 ± 0.9 % lower than the reference LAS. 99.6 % of the values fit the trend line.

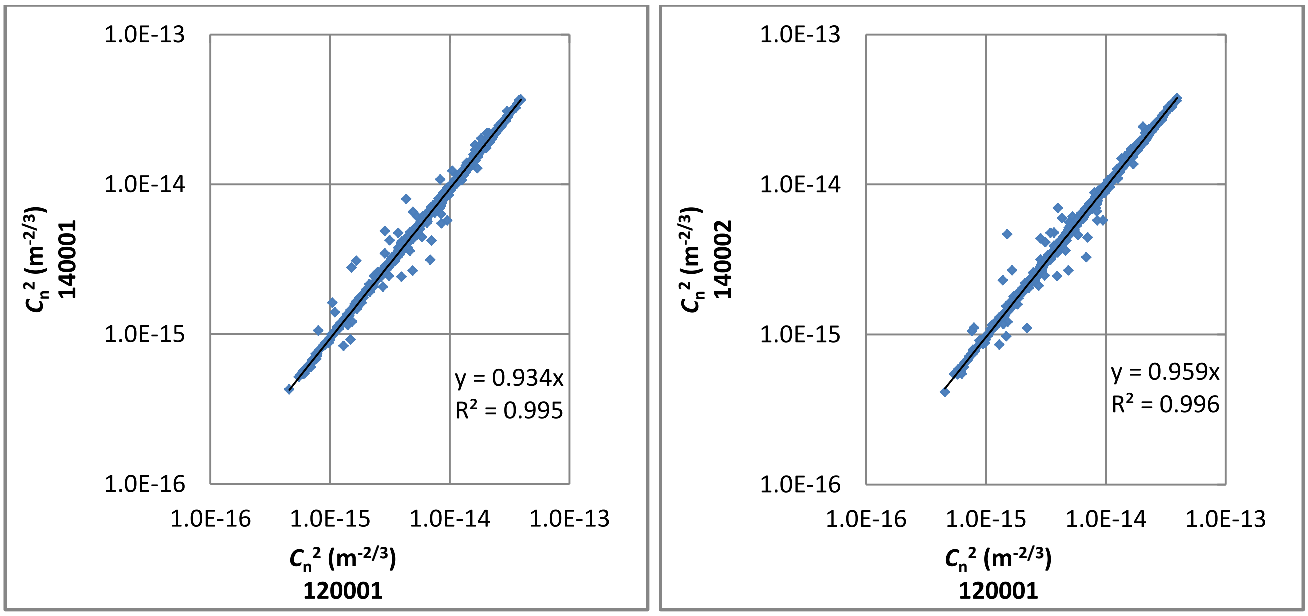

Figure 25: Scatterplots of left XLAS 140001 as function of LAS 120001 and right XLAS 140002 as function of LAS 120001

Table 9, in Appendix E: Results comparison 1 April – 25 May, shows the slope and the R^2 of the structure parameter of the refractive index for XLAS 140001 as a function of LAS 120001 for different time periods. In this period the values fit the line at least within 97.4 % and the mean of the slope is 0.941 ± 0.007. This means that XLAS 140001 measures 6.3 ± 0.7 % lower values than LAS 120001 over a period of two months.

Table 10, in Appendix E: Results comparison 1 April – 25 May, shows the slope and the R^2 of the structure parameter of the refractive index for XLAS 140002 as a function of LAS 120001 for different time periods. In this period the values fit the line at least within 97.5 % and the mean of the slope is 0.960 ± 0.009. This means that XLAS 140002 measures 4.2 ± 0.9 % lower values than LAS 120001 over a period of two months.

Figure 26 shows the structure parameter of the refractive index of XLAS 140002 as function of the structure parameter of the refractive index of 140001. The slope of the scatterplot is equal to 1.025 ± 0.009, which means 140002 measures 2.5 ± 0.9 % higher values than 140001. 99.7 % of the values fit the trend line.

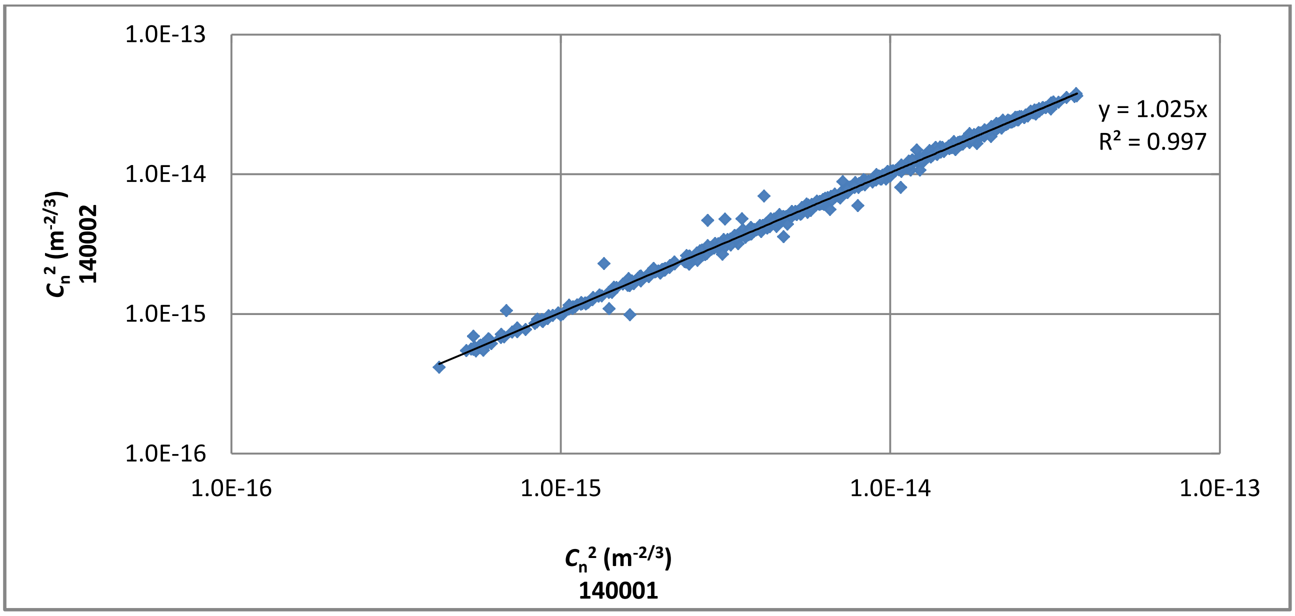

Figure 26: XLAS 140002 as function of XLAS 140001

Table 11, in Appendix E: Results comparison 1 April – 25 May, shows the slope and the R^2 of the structure parameter of the refractive index for XLAS 140002 as a function of XLAS 140001 for different time periods. In this period the values fit the line at least within 97.0 % and the mean of the slope is 1.013 ± 0.009. This means that XLAS 140002 measures 1.3 ± 0.9 % higher values than XLAS 140001 over a period of two months.

4.3 Comparison between Kipp LAS and WagLAS

The data which is used for the comparison is over the period from 13 May to 16 May. These days are chosen because of the low incidence of precipitation. The days for the comparison constrained by using the data of the meteorological instruments. The meteorological data is shown in Appendix C: Meteorological data , where Figure 34 shows the temperature, Figure 35 shows the pressure, Figure 36 shows the wind speed and Figure 37 shows the net radiation. The humidity sensor was damaged during this period, so the humidity values are not shown. From the net radiation data it can be concluded that there were some clouds in this period. The temperature in this period was around 15 ^{o}C. There is one dip in the temperature on 14 May, this is a result of a rain shower.

The Wageningen LAS has a band pass filter from 0.1 Hz to 400 Hz. The Kipp & Zonen LAS has a band pass filter from 0.5 to 400 Hz. With low crosswind speed the frequency spectrum shifts to the left, so then the Wageningen LAS measures more scintillations than the Kipp & Zonen LAS.

Figure 27 shows the received signal as function of the time from 13 to 16 May. Each data point is an average of a 10 minute interval. The received signal on 120001 and 120002 are nearly the same. The received signal on the Wageningen LAS is smaller than the Kipp LAS. On 13 and 14 May at 18:00 UTC time, 20:00 local Dutch time, the sun is shining into the detector of the Kipp LAS. This leads to an error in the data, so this period was deleted from the data. The Wageningen LAS (WAG) has an dip on the night and early morning of 15 May. This can be a result of a fogged window, because the Wageningen LAS has no heating capability for the window or instrument.

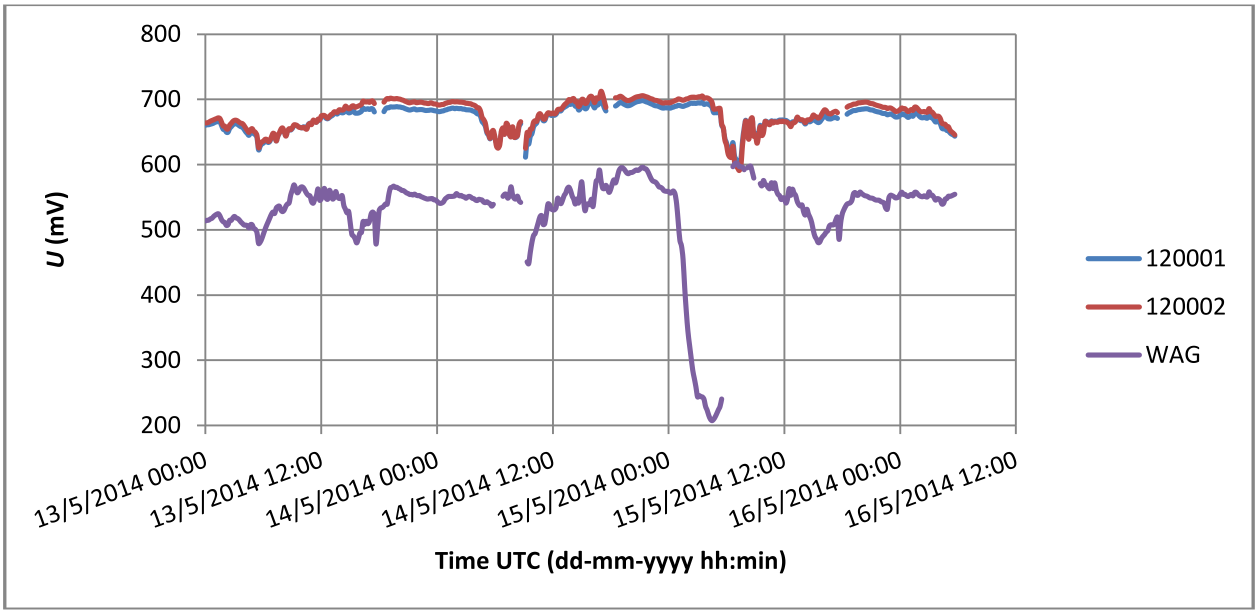

Figure 27: The received signal as function of time for the Wageningen LAS and LAS 120001 and 120002

Figure 28 shows the structure parameter of the refractive index as a function of the time. The parameter drops around sunrise and sunset. The parameter measured by the Wageningen LAS is higher than the parameter measured by Kipp LAS 120001 and 120002.

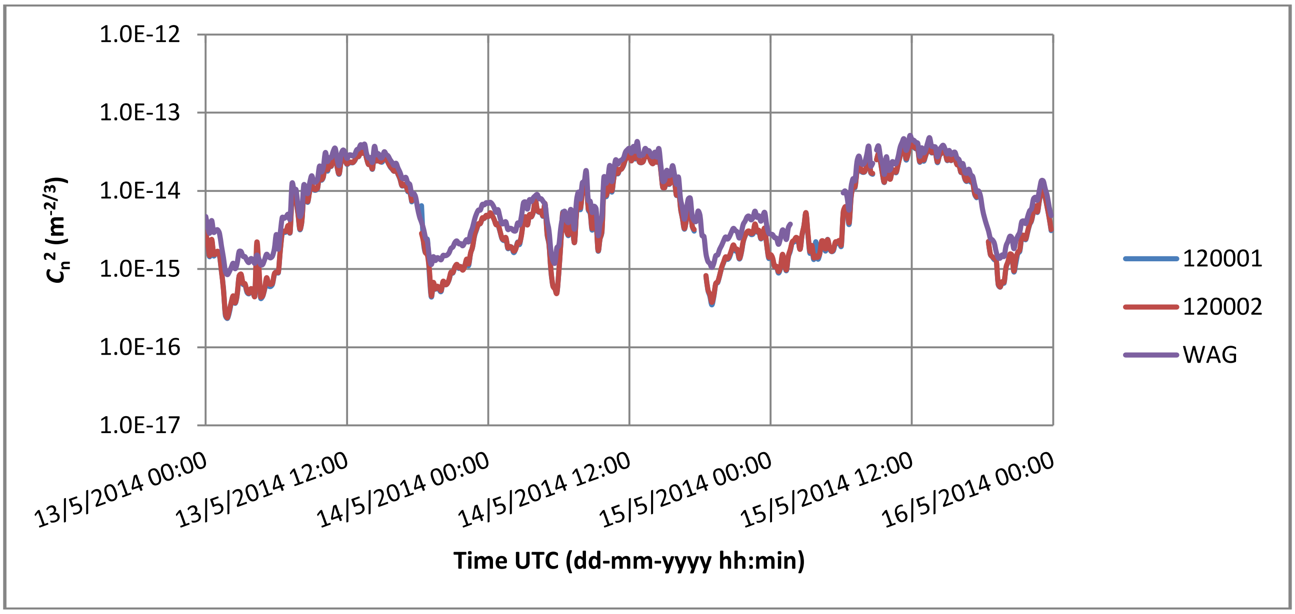

Figure 28: The structure parameter of the refractive index as function of time for the Wageningen LAS and LAS 120001 and 120002

Figure 29 shows the structure parameter of the refractive index of LAS 120002 as a function of the structure parameter of the refractive index of LAS 120001. The slope of the scatterplot is 1.029 ± 0.005, which means that 120002 measures 2.9 ± 0.5 % higher values than 120001. The difference between the reference and the control receiver is small enough to compare LAS 120001 with the BLS. 99.9 % of the values fit the trend line.

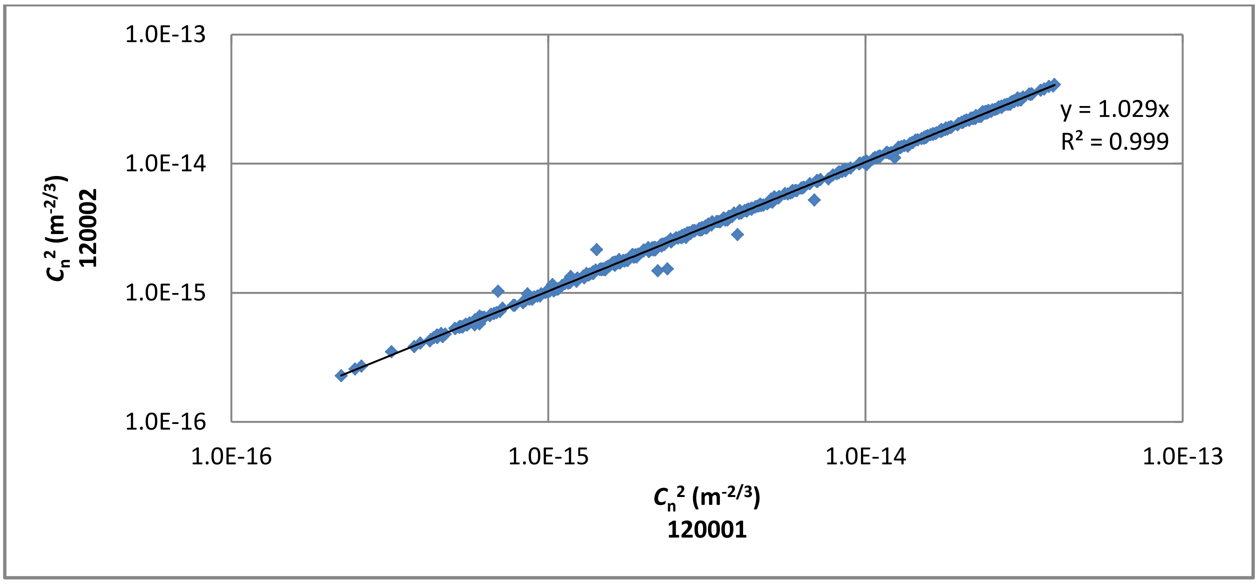

Figure 29: LAS 120002 as function of LAS 120001

Figure 30 shows the structure parameter of the refractive index of the Wageningen LAS as a function of the structure parameter of the refractive index of Kipp LAS 120001. The red line is 1:1 line and the black line is the trend line through the scatterplot. The slope of the scatterplot is 1.23 ± 0.02.Which means that the Wageningen LAS measures 23 ± 2 % higher values than the Kipp LAS. Below 5.0 x 10^{-15} $m^{-2/3}$ the slope of the scatterplot diverges from the fitted slope to horizontal. Therefore the Wageningen LAS does not measure lower values than 5.0 x 10^{-16} $m^{-2/3}$. Noise in the signal could be the reason for this, due to a stronger electronic amplification factor in this instrument. This can be seen as a noise spike in the frequency spectrum of the Wageningen LAS shown in Figure 19.

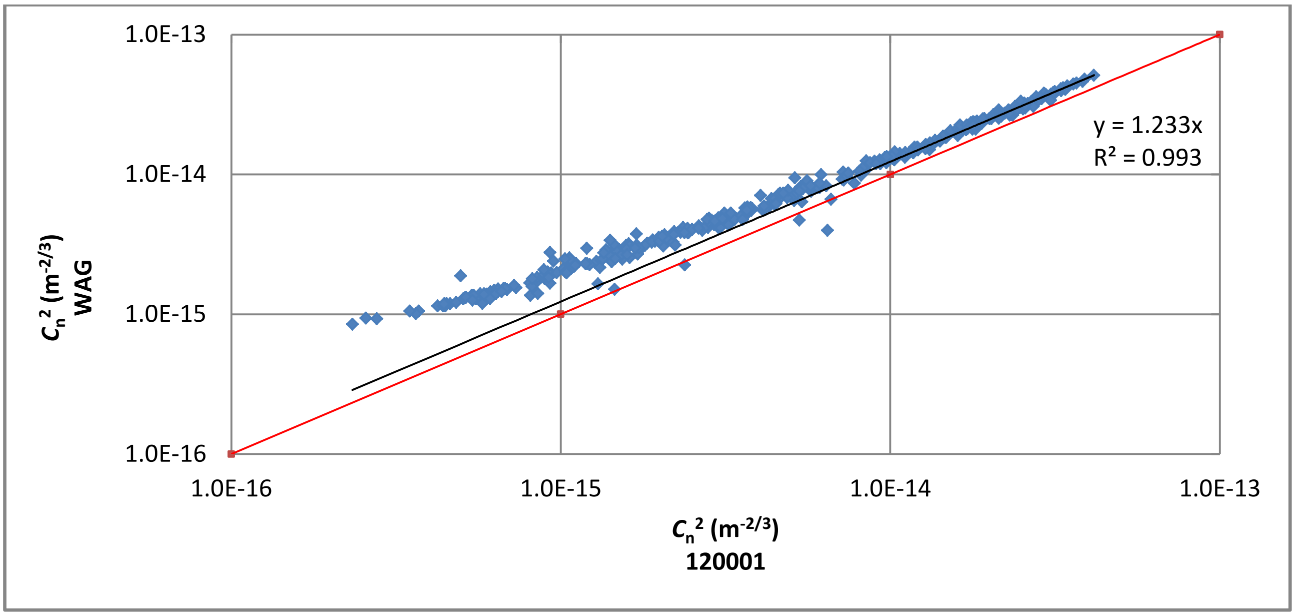

Figure 30: The Wageningen LAS as function of Kipp LAS 120001

4.4 Comparison between LAS and Scintec LAS

The LAS was compared with the Scintec LAS (BLS900). The data which was used for the comparison are from 16 May to 20 May. These days are chosen because of the dry and warm weather, and employing data from the meteorological instruments. The meteorological data is shown in Appendix D: Meteorological data 15 – 20 May, where Figure 38 shows the temperature, Figure 39 shows the pressure, Figure 40 shows the wind speed and Figure 41 shows the net radiation. The humidity sensor was damaged during this period, therefore the humidity values are not shown. From the net radiation data it can de concluded that the first and the last day in this period were slightly cloudy. The temperature during this period increased every day by 2 ^{o}C.

The BLS900 has a low pass filter of 150 Hz. The LAS has a band pass filter from 0.5 to 400 Hz. With low crosswind, the frequency spectrum shifts to the left, so then the BLS900 measures more scintillations than the LAS. The band pass filter settings on LAS 040007 are changed for this comparison period to a range of 0.1 Hz to 400 Hz.

The BLS900 does not log the received signal over a 10 minute average. Therefore the received signal on the LAS cannot be compared with the received signal on BLS900. Figure 31 shows the structure parameter of the refractive index as function of the time. The parameter drops around sunrise and sunset and gets stable during the night.

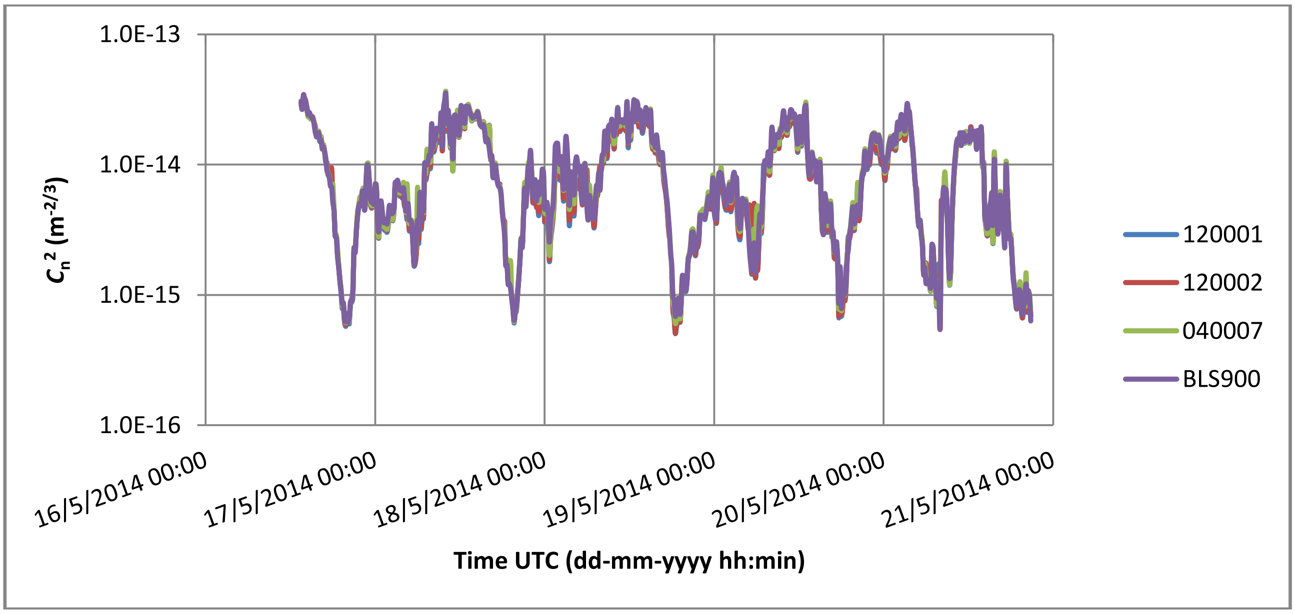

Figure 31: The structure parameter of the refractive index as function of time

The comparison between LAS 120001 and LAS 120002 is shown in paragraph 4.2 in Figure 24. The difference between the reference and the control receiver is small enough to compare LAS 120001 with the BLS. Figure 32 shows the structure parameter of the refractive index of the BLS900 as a function of the structure parameter of the refractive index of LAS 120001. The slope of the scatterplot is equal to 1.08 ± 0.01, which means that BLS900 measures 8 ± 1 % higher values than the LAS 120001. 98.2 % of the values fit the trend line.

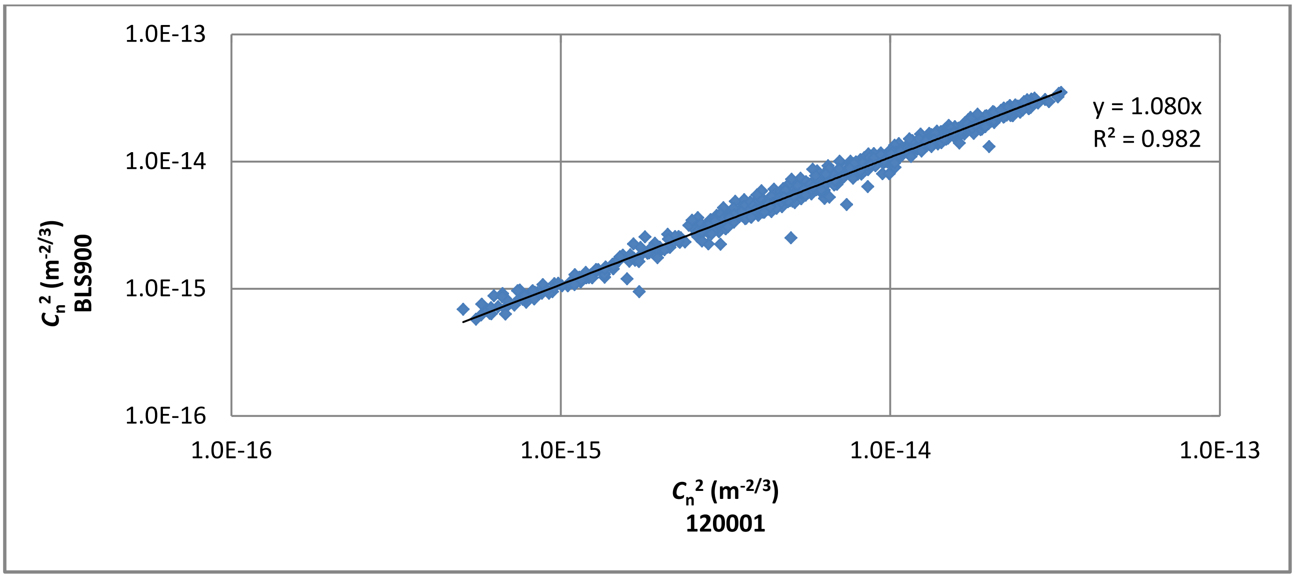

Figure 32: The BLS900 as function of LAS 120001

Table 12, in Appendix E: Results comparison 1 April – 25 May, shows the slope and the R^2 of the structure parameter of the refractive index for LAS 040007 as a function of LAS 120001 for different time periods. There results correspond to a band pass filter of 0.5 Hz to 400 Hz. In this period the values fit the line at least within 97.6 % and the mean of the slope is 1.000 ± 0.007. This means that LAS 040007 measures the same values as LAS 120001 over a period of two months. Therefore LAS 040007 can be used as a reference with other filter settings for the comparison against the BLS.
Figure 33 shows the structure parameter of the refractive index of the BLS900 as a function of the structure parameter of the refractive index of LAS 040007. The slope of the scatterplot is equal to 1.02 ± 0.01, which means that the BLS900 measures 2 ± 1 % higher values than LAS 040007. 98.9 % of the values fit the trend line. Therefore the BLS900 measures 8 ± 1 % higher values than the LAS with a band pass filter of 0.5 Hz to 400 Hz and the BLS900 measures 2 ± 1 % higher values than the LAS with a band pass filter of 0.1 Hz to 400 Hz.

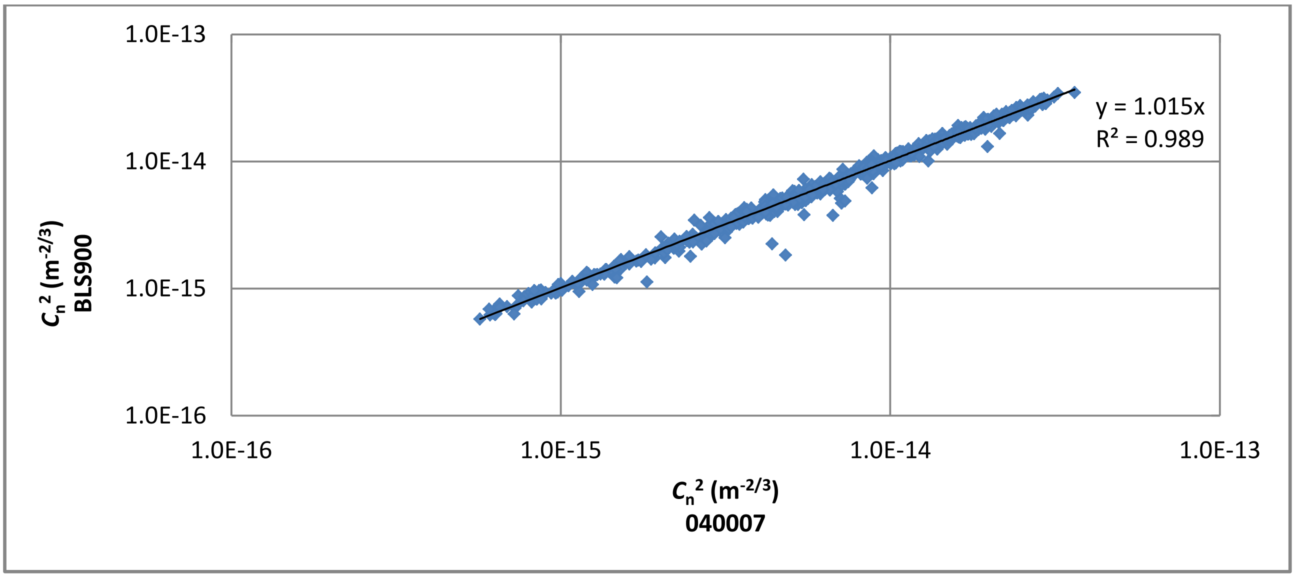

Figure 33: The BLS900 as function of LAS 040007

5 Conclusion

The raw frequency spectrum of the LAS and the XLAS with reduced aperture have the same typical scintillation spectrum. The Wageningen LAS shows a high spike around 155 Hz and some small spikes around 33 and 35 Hz. These noise spikes influence the calculated C_{n}^2, because the area under the curve is proportional to C_{n}^2.

Control LAS 120002 measures 2.8 ± 0.5 % higher C_{n}^2 than the reference LAS 120001. For further research the control LAS can be multiplied with a factor of 0.972, so the control and the reference LAS indicate the same value, for ease of use in further calibrations.
XLAS 140001 measures 6.3 ± 0.7 % lower C_{n}^2 than reference LAS 120001, with a little scatter. XLAS 140002 measures 4.2 ± 0.9 % lower C_{n}^2 than reference LAS 120001, with a little scatter. XLAS 140002 measures 1.3 ± 0.9 % higher C_{n}^2 than XLAS 140001, with a little scatter. The lower measured C_{n}^2 by the XLAS in comparison to the LAS can be a result of:

- A different lens with a longer focal length in the XLAS can result in a smaller focus spot for the XLAS in comparison to the LAS.
- The effective diameter of the LAS is around 0.149 m, but due to different ring sizes inside the LAS the physical clear aperture can be around 1 mm smaller or larger.

The Wageningen LAS measures 23 ± 2 % higher C_{n}^2 than reference LAS 120001. The noise peak in the frequency spectrum leads to an offset in the measured C_{n}^2. When C_{n}^2 decreases the influence of the peak increases. The detector in the Wageningen LAS is optimised for using at path lengths longer than 1.5 km. A new comparison has been started on 25 May with a more suitable detector in the Wageningen LAS, but data collection is on-going.

LAS 040007 measures the same values of C_{n}^2 as reference LAS 120001 within an uncertainty of 0.8 % and with the band pass filter settings of 0.5 Hz to 400 Hz, with a little scatter.
The BLS900 measures 8 ± 1 % higher C_{n}^2 than reference LAS 120001 and the BLS900 measures 2 ± 1 % higher C_{n}^2 than LAS 040007 with a band pass filter of 0.1 Hz to 400 Hz, with a good fit. Therefore the BLS900 measures within a difference of 2 % the same values as the LAS with a band pass filter of 0.1 Hz to 400 Hz. With a band pass filter of 0.5 Hz to 400 Hz the LAS measures 6 % lower values than with a band pass filter of 0.1 Hz to 400 Hz, so 6 % of the scintillation is lost. The band pass filter settings on the LAS and XLAS need to be set to 0.1 Hz to 400 Hz to avoid missing data.

The XLAS was not tested over a distance of 10 km, but so far only over a distance of 889 m.

6 Recommendations for the future

In the specifications for the old MkI XLAS it is stated that the XLAS measures over an open path up to a distance of 10 km. Therefore the XLAS still needs to be tested over a distance of 10 km, to determine the maximum range. Also the minimum range need to determined.

The effective aperture diameter of the LAS and the XLAS are not known accurately. The physical diameter of the LAS aperture is 149 mm and the physical diameter of the XLAS lens aperture is 328 mm. The reduction ring has an aperture diameter of 150 mm. Due to overlapping rings inside the LAS with different tolerances, the effective aperture diameter can be smaller than the physical aperture. Therefore the effective diameter of the LAS and the XLAS need to be investigated to calculate the structure parameter of the refractive index correctly. The effective diameter can be measured by measuring the received signal as function of different sizes of reduction rings in front of the LAS.

The Fresnel lens in the XLAS is different than the Fresnel lens in the LAS. The focal length of the Fresnel lens in the XLAS is more than two times longer than the focal length in the LAS. Due to this difference, the focus spot could be different for both Fresnel lenses. The spot size of the Fresnel lens would be smaller if the focal length is larger. Therefore the quality of the focus, spot size and shape, need to be determined.

A LAS with a band pass filter of 0.1 Hz to 400 Hz measures 6 % higher C_n^2 values than a LAS with a band pass filter of 0.5 Hz to 400 Hz. The band pass filter settings on the LAS and XLAS need to be set to 0.1 Hz to 400 Hz as a standard to improve the instrument measurement.

7 List of abbreviations and units

The definition and the unit of the symbols are explained in Table 7.

Table 7: The definition and the symbol of the units used

Symbol	Definition	Unit
A_{Q}	Constant of humidity	-
A_{T}	Constant of temperature	-
b	Sensible convection limit, 0.48	-
C_{n}^{2}	Structure parameter of the refractive index of air	$m^{-2/3}$
c_{p}	Heat capacity of air	J/kgK
C_{Q}	Structure parameter of humidity	$kgm^{-3}m^{-2/6}$
C_{T}	Structure parameter of temperature	$Km^{-2/6}$
C_{TQ}	Structure parameter of temperature and humidity	$Kkgm^{-3}m^{-2/3}$
D	Effective aperture diameter of the XLAS	m
d	Zero displacement height	m
d_1	Distance from the LED to the LED back plate	mm
e	Constant, 1.12	-
f	Focal length	mm
f_{req}	Frequency	Hz
g	Gravitational acceleration	m/s^2
G_{s}	Soil heat flux	W/m^2
H	Sensible heat flux	W/m^2
H_{free}	Sensible heat flux from the free convection method	W/m^2
L	Path length between the transmitter and receiver	m
l_0	Minimum eddy size	m
L_0	Maximum eddy size	m
$L_V E$	Latent heat flux	W/m^2
LW_{in}	Long wave incoming solar radiation	W/m^2
LW_{out}	Long wave outgoing earth radiation	W/m^2
m_1	Wavelength dependent constant,	K/Pa
m_2	Wavelength dependent constant,	K/Pa
n	Refractive index	-
N	Number of data points	-
P	Pressure	Pa
Q	Absolute humidity	kg/m^3
R_1	Radius of curvature of the convex side of the lens	mm

R_2	Radius of curvature of the flat side of the lens	mm
R_n	Net radiation	W/m^2
R_V	Specific gas constant for water vapour	J/kgK
R^2	R^2 function of excel	-
s	Slope of the scatter plot	-
SW_{in}	Short-wave incoming solar radiation	W/m^2
SW_{ref}	Short-wave reflected solar radiation	W/m^2
T	Temperature	K
u	Normalized position	-
U_{ave}	Averaged voltage over 5 s	mV
U_{var}	Variance in amplitude	mV
x	Distance from the transmitter	m
z	Effective height of the beam	m
β	Bowen ratio	-
λ	Wavelength	m
ρ	Density of air	kg/m^3
$\sigma_{\ln I}$	Variance of intensity fluctuations	-

8 References

[1] Meijninger, W.M.L., *Surface fluxes over natural landscapes using scintillometry*, CIP-data koninklijke bibliotheek, Wageningen, 2003

[2] van Kersteren, J.H., *Measuring water-vapour and carbon-dioxide Fluxes at field scales with scintillometry*, Wageningen, 2012

[3] Giancoli, Douglas C., *Natuurkunde 2, Elektriciteit magnetisme optica modern fysica*, druk 4, Pearson Benelux, , 2009

[4] http://okfirst.mesonet.org/train/meteorology/EnergyBudget2.html

[5] http://pmm.nasa.gov/education/lesson-plans/global-energy-budget

[6] http://www.kippzonen.com/Product/193/LAS-MkII-Scintillometer#.Uz1AgqiSzeA

[7] http://www.edmundoptics.eu/technical-resources-center/optics/advantages-of-fresnel-lenses/

[8] http://en.wikipedia.org/wiki/Sellmeier_equation

[9] http://refractiveindex.info/?shelf=organic&book=poly(methyl_methacrylate)&page=Szczurowski

[10] http://earthobservatory.nasa.gov/Features/EnergyBalance/

[11] http://www.thorlabs.com/newgrouppage9.cfm?objectgroup_id=1000

[12] http://www.farnell.com/datasheets/423255.pdf

[13] http://www.scintec.com/english/Web/Scintec/Details/A012000.aspx

Appendix A: Assignment description (Dutch)

De opdracht is om een extra grote scintillometer (XLAS) te bouwen en te testen. Een scintillometer is een instrument waarmee de verandering van de brekingsindex van de lucht gemeten kan worden. Door de opstijgende lucht van bijvoorbeeld een asfaltweg op een warme dag, zal de brekingsindex van de lucht fluctueren. Deze fluctuaties zijn een maat voor de opstijgende warmte. De scintillometer bestaat uit een zender en een ontvanger. De zender bevat een LED die licht uitzendt met een golflengte van 850 nm en wordt ontvangen door de detector op een bepaalde afstand.
De huidige scintillometer (LAS) heeft een bereik tot 4,5 km. De extra grote scintillometer (XLAS) moet een bereik krijgen van 10 km. Het testen van de XLAS zal gedeeltelijk binnen en gedeeltelijk buiten op het dak van het bedrijf plaatsvinden. Ook zal er getest worden op de KNMI meetmast bij Cabauw.

Appendix B: Sample equations

Sample equation 4 determined the refractive index at a wavelength of 632 nm from equation 14,

$$n = \sqrt{1 + \frac{B_1\lambda^2}{\lambda^2 - C_1} + \frac{B_2\lambda^2}{\lambda^2 - C_2} + \frac{B_3\lambda^2}{\lambda^2 - C_3}} \tag{14}$$

where,

$\lambda = 632.0 \text{ nm}$
$B_1 = 0.9965$
$B_2 = 0.1896$
$B_3 = 0.004110$
$C_1 = 7.870 \text{ x } 10^{-15} \text{ nm}^2$
$C_2 = 2.191 \text{ x } 10^{-14} \text{ nm}^2$
$C_3 = 3.857 \text{ x } 10^{-12} \text{ nm}^2$

so that,
$n = 1.489$

Sample equation 5 determined the focal length at a wavelength of 632 nm and a refractive index of 1.489 from equation 15,

$$f = \frac{1}{(n-1)\left(\frac{1}{R_1} - \frac{1}{R_2}\right)} \tag{15}$$

where,

$n = 1.489$
$R_1 = 275.5 \text{ mm}$
$R_2 = 1.000 \text{ x } 10^{10} \text{ mm}$

so that,
$f = 563.5 \text{ mm}$

Appendix C: Meteorological data 13 – 16 May

This appendix shows the meteorological data from 13 May to 16 May. Figure 34 shows the temperature as function of the time, measured at two heights of 0.5 m and 2.5 m. Figure 35 shows the pressure as function of the time. Figure 36 shows the wind speed as function of the time. Figure 37 shows the net radiation as function of the time.

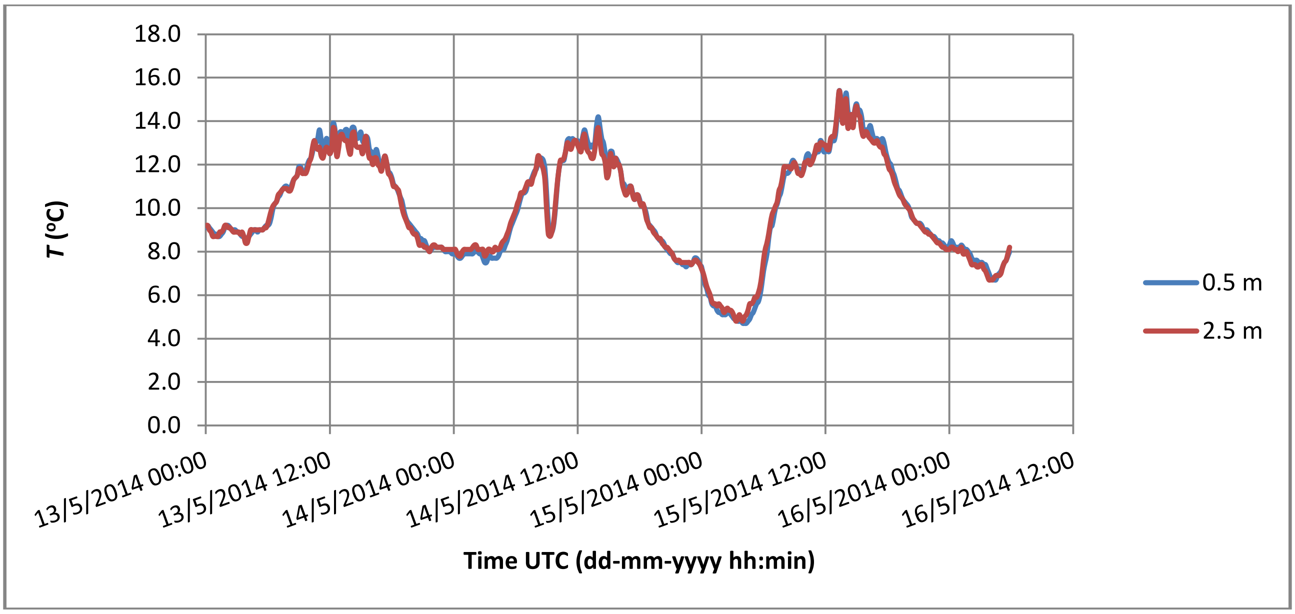

Figure 34: The temperature as function of time, measured at a height of 0.5 m and 2.5 m

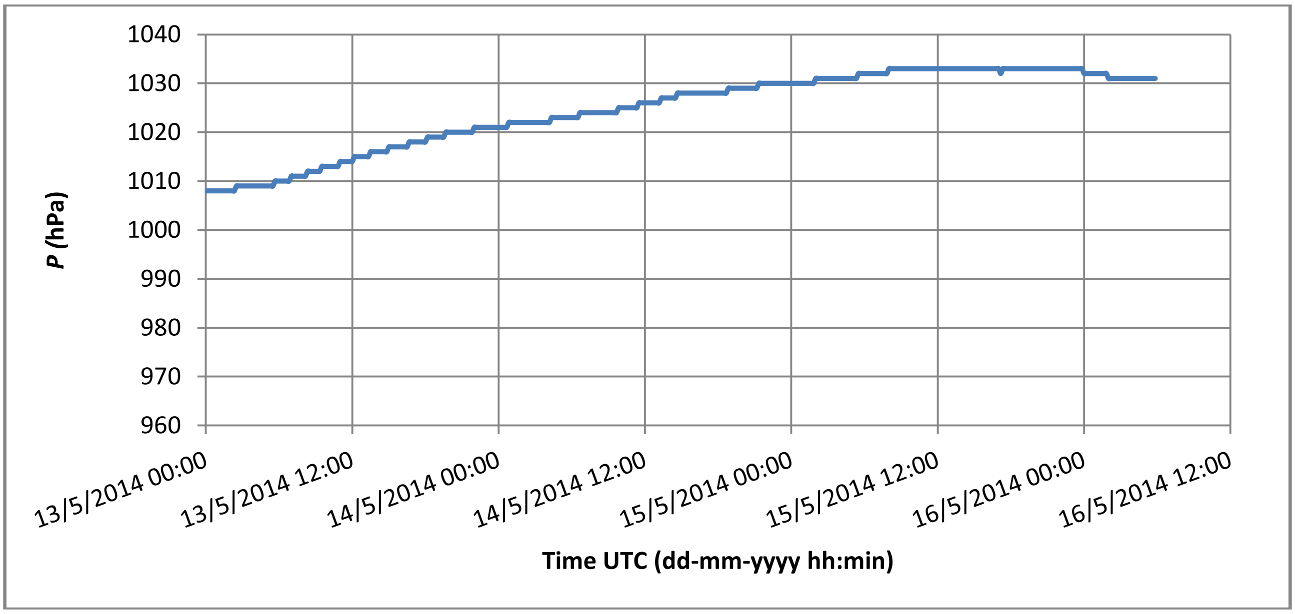

Figure 35: The pressure as function of time

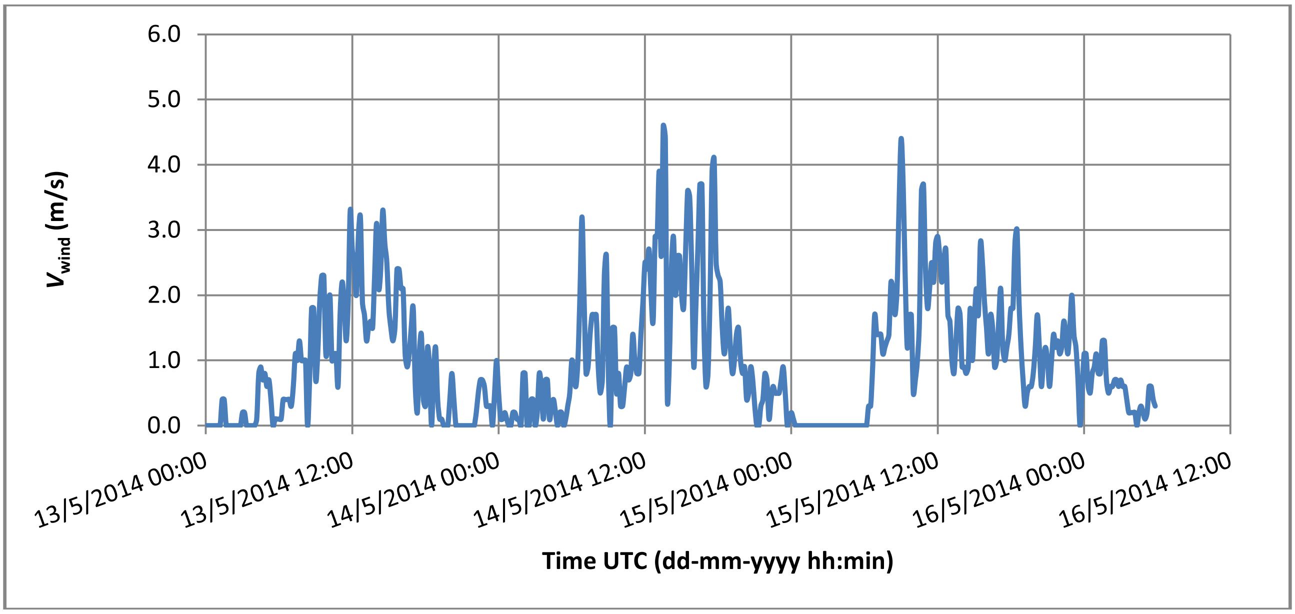

Figure 36: The wind speed as function of time

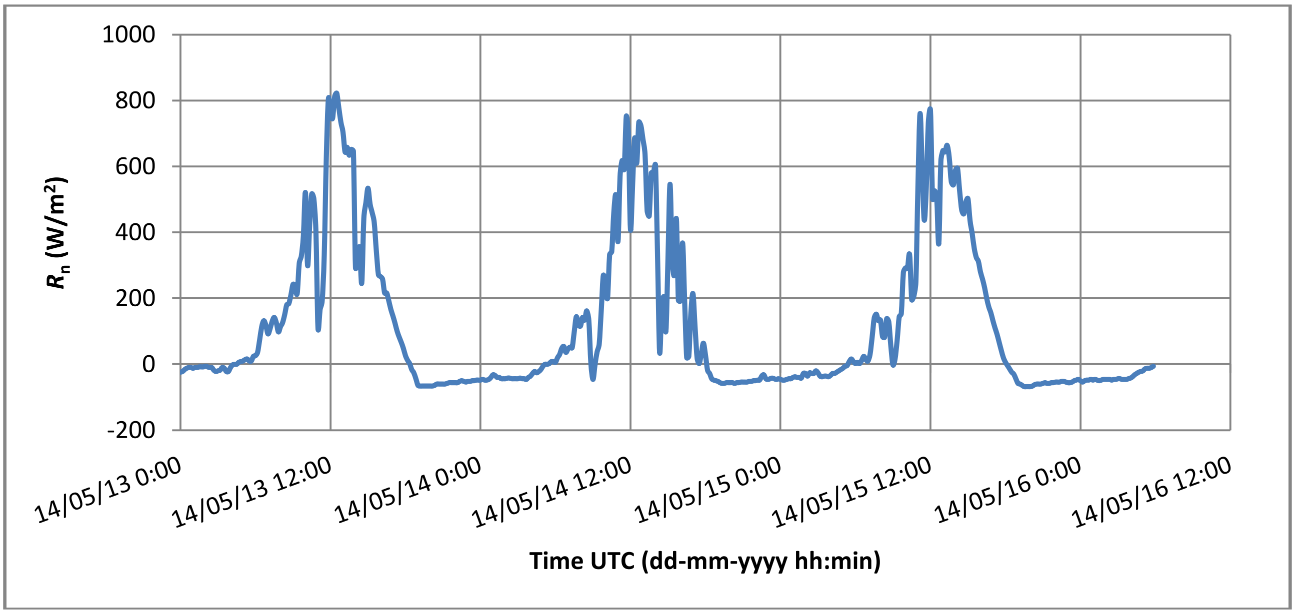

Figure 37: The net radiation as function of time

Appendix D: Meteorological data 15 – 20 May

This appendix shows the meteorological data from 15 May to 19 May. Figure 38 shows the temperature as function of the time, measured at two heights of 0.5 m and 2.5 m. Figure 39 shows the pressure as function of the time. Figure 40 shows the wind speed as function of the time. Figure 41 shows the net radiation as function of the time.

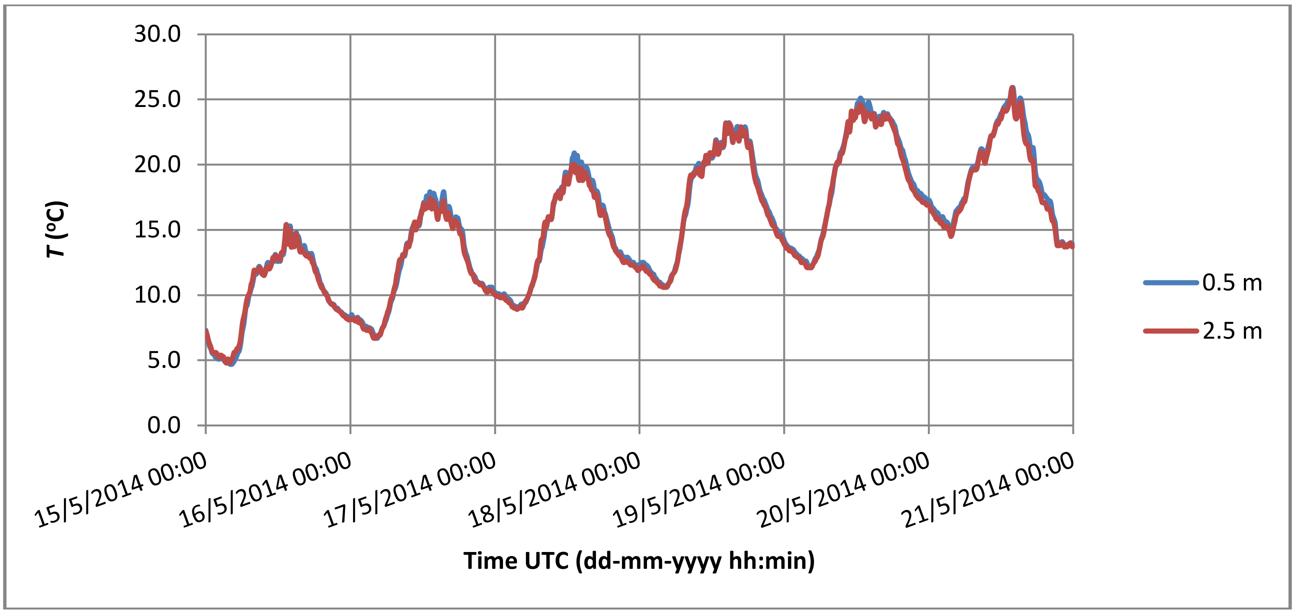

Figure 38: The temperature as function of time, measured at a height of 0.5 m and 2.5 m

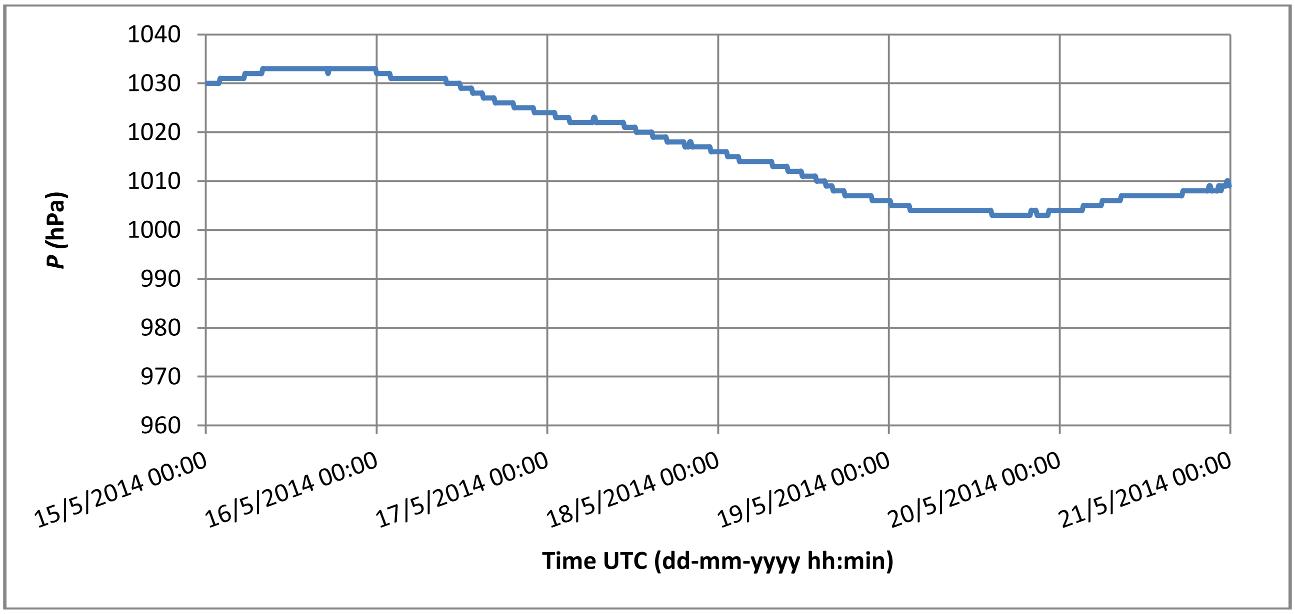

Figure 39: The pressure as function of time

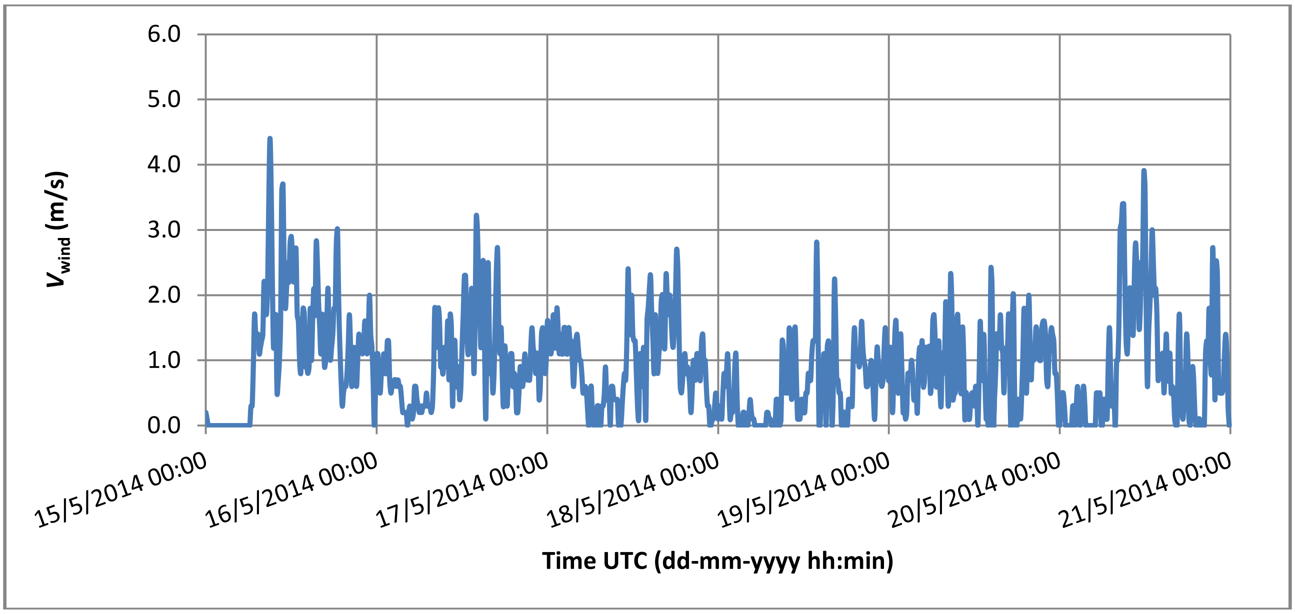

Figure 40: The wind speed as function of time

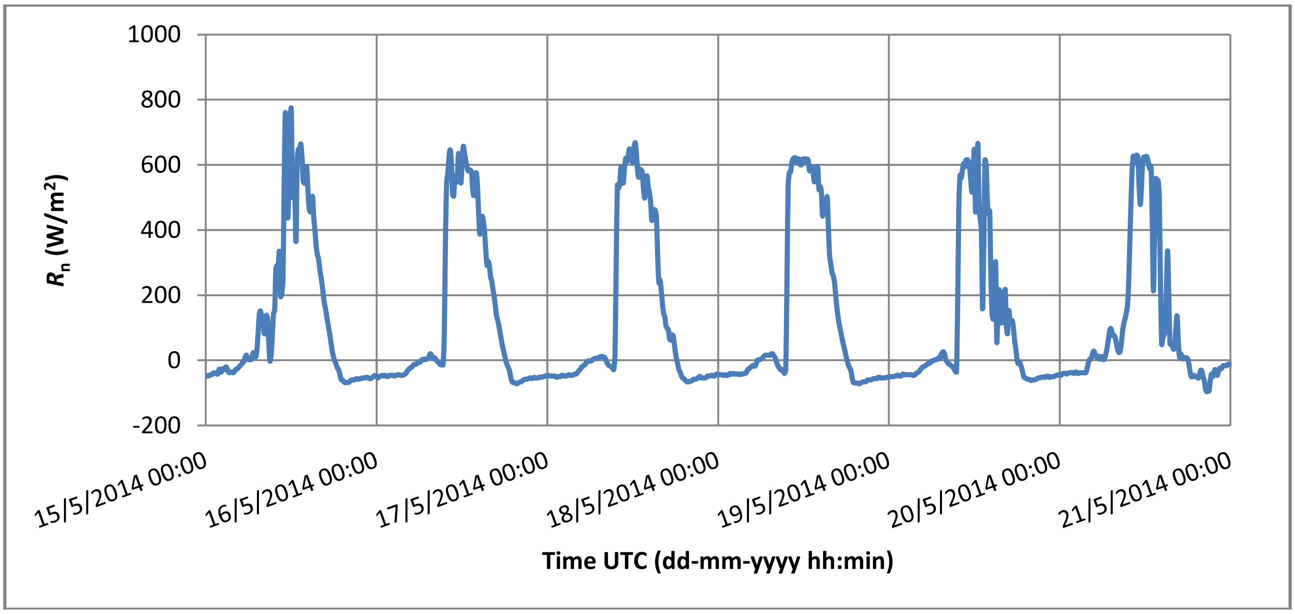

Figure 41: The net radiation as function of time

Appendix E: Results comparison 1 April – 25 May

This appendix shows the number of data points (*N*), the slope (*s*) and the R^2 of the structure parameter of the refractive index for one LAS as a function of another LAS for different time periods. Table 8 shows control LAS 120002 as a function of reference LAS 120001, Table 9 shows XLAS 140001 as a function of reference LAS 120001, Table 10 shows XLAS 140002 as a function of reference LAS 120001, Table 11 shows XLAS 140002 as a function of XLAS 140001 and Table 12 shows LAS 040007 as a function of reference LAS 120001. The uncertainty in the slope is calculated from the LINEST function in Excel.

Table 8: Control LAS 120002 as a function of reference LAS 120001 for different time periods with the number of data points (*N*), the slope (*s*), and the R^2.

Date	*N* (-)	*s* (-) ± 0.002	R^2 (-)
1-5 April	658	1.031	0.997
9-13 April	664	1.031	0.998
14-16 April	396	1.017	0.988
18-22 April	626	1.029	0.995
25-27 April	415	1.030	0.996
2-6 May	697	1.028	0.997
15-19 May	706	1.032	0.999
Mean slope		1.028 ± 0.005	

Table 9: XLAS 140001 as a function of reference LAS 120001 for different time periods

Date	*N* (-)	*s* (-) ± 0.002	R^2 (-)
1-5 April	658	0.932	0.984
9-13 April	664	0.945	0.993
14-16 April	396	0.945	0.988
18-22 April	626	0.944	0.974
25-27 April	415	0.952	0.979
2-6 May	697	0.938	0.990
15-19 May	706	0.934	0.995
Mean slope		0.941 ± 0.007	

Table 10: XLAS 140002 as a function of reference LAS 120001 for different time periods

Date	*N* (-)	*s* (-) ± 0.002	R^2 (-)
9-13 April	664	0.966	0.995
14-16 April	396	0.949	0.977
18-22 April	626	0.955	0.975
25-27 April	415	0.976	0.985
2-6 May	697	0.954	0.991
15-19 May	706	0.959	0.996
Mean slope		0.960 ± 0.009	

Table 11: XLAS 140002 as a function of XLAS 140001 for different time periods

Date	*N* (-)	*s* (-) ± 0.002	R^2 (-)
9-13 April	664	1.019	0.994
14-16 April	396	1.003	0.985
18-22 April	626	1.004	0.970
25-27 April	415	1.008	0.977
2-6 May	697	1.016	0.996
15-19 May	706	1.025	0.997
Mean slope		1.013 ± 0.009	

Table 12: LAS 040007 as a function of reference LAS 120001 for different time periods

Date	*N* (-)	*s* (-) ± 0.002	R^2 (-)
1-5 April	658	1.001	0.985
9-13 April	664	1.008	0.988
14-16 April	396	0.989	0.976
18-22 April	626	0.999	0.981
25-27 April	415	1.009	0.987
2-6 May	697	0.993	0.989
Mean slope		1.000 ± 0.008	